FACULTY OF SCIENCE AND TECHNOLOGY

MASTER'S THESIS

Study program/specialization: Marin and offshore technology	The *spring* semester, *2023* Open
Author: Oskar Sande	Oskar Sande
Supervisor at UiS: Professor Yihan Xing	
Thesis title: Design and analysis of a hybrid timber-steel floating substructure for a 15 MW TLP-type FWT.	
Credits (ECTS): 30	
Keywords: Tension leg platform Wind turbine Static analysis Pontoon design Wood Glulam	Pages: 75 + appendix: 4 Stavanger, *13.06.2023*.

Contents

Table of Figures

List of tables:

Abstract

Offshore wind has been an important topic for harvesting renewable energy in the last few years. Due to the low terrain roughness and large area, offshore wind is very attractive. This thesis provides the concept design for a hybrid steel/ glulam tension leg platform to support the IEA 15MW wind turbine. Pontoon design is a significant part of the thesis, starting from a base model, upscaling, and finalizing the design with a structural analysis. The base parameters are calculated using Microsoft Excel and then Ansys Mechanical to create and analyse the FEM- model. The result of the analysis gives confidence in the concept design.

Nomenclature

Turbine

f_{1p} , f_{3p}	Turbine rotation frequency
Soft- soft, soft-stiff and stiff- stiff	Reference to the placing of the foundational eigenfrequency

Expressions

SWL	Still water level
c/s	Cross-section
cc	Centre to centre

ULS timber

M_{Ed}	design moment
M_{Rd}	Moment capacity
V_{Ed}	Design Shear force
V_{Rd}	Shear capacity
q_d	Design load
$\sigma_{t,0,d}$	Design tension stress
$\sigma_{m,y,d}, \sigma_{m,z,d}$	Design bending stress about the principal axis
$\sigma_{crit,m}$	Critical design stress
l	Element length
l_{eff}	Effective length
b_{eff}	Effective width
A	Cross-sectional area
$f_{m,d}$	Design bending strength
$f_{m,k}$	Material bending strength
$f_{m,g,k}$	Deflection
$f_{m,0,g,k}$	Parallel tension strength
$f_{m,90,g,k}$	Tension strength
$f_{v,d}$	Design shear strength
$f_{v,k}$	Material shear strength
k_h	Depth factor
$f_{t,0,d}$	Design tension strength along the grain
$f_{c,0,d}$	Design compressive strength along the grain
$f_{m,y,d}$, $f_{m,z,d}$	Design bending strength about the principal axis.
$k_{c,z}$	Instability factor
k_m	
k_z	
k_{mod}	Modification factor for the duration of load and moisture content.
k_{cr}	The crack factor for shear resistance
k_{crit}	
γ_M	The partial factor for material properties, also accounting for model uncertainties and dimensional variations.
W	Section modulus
R	Radius of gyration

$E_{0,g,mean}$	Modulus of elasticity
$E_{90,g,mean}$	Modulus of elasticity, parallel
$E_{0,05}$	Fifth- percentile modulus of elasticity
$G_{g,mean}$	Shear modulus
$\lambda_{rel,m}$	Relative slenderness ratio corresponding to bending
$\lambda_{rel,z}$	Relative slenderness ratio about z-axis
λ_z	Slenderness ratio

ULS Steel

b	Appropriate width taken from table 5.2 of EN 1993-1-1
t	plate thickness
A_{eff}	Effective cross-section area.
A_s	Cross-sectional area of steel plate.
E	Elastic modulus
$e_{y,N}, e_{z,N}$	Shift in the position of neutral axis, the eccentricities with respect to neutral axis.
$W_{y,eff}, W_{z,eff}$	Effective elastic section modulus with respect to its axis.
ψ	Stress ratio
ε	Material strength ratio
k_σ	Buckling factor corresponding to the stress ratio ψ and boundary conditions
N_{Ed}	Design axial force.
$M_{y,Ed}, M_{z,Ed}$	Design bending moment with respect to $y-y$ and $z-z$ axis
$\sigma_{cr,p}$	Elastic critical plate buckling stress.
$\sigma_{cr,c}$	Elastic critical column buckling stress.
X_c	Reduction factor due to column buckling.
γ_{M0}	Partial factor
ρ	Reduction factor due to plate buckling.
ρ_{red}	Reduction factor for plate buckling
λ_p	Relative slenderness
v	Poisson's ratio
ζ	Buckling stress ratio

Hydrostatic

σ_w	Hydrostatic pressure
ρ	Water density
H	Distance from SWL
$a_t[D]$	Transverse added mass per unit length
$a_t[H]$	
A_{ij}	Added mass
θ_i	Pontoon angle
n_p	Number of pontoons
l_p	Pontoon length
k_{ii}	System stiffness

Chapter 1 Introduction

1.1. General background

Moving away from filthy, non-renewable energy sources is becoming more and more critical. Renewable energy considerably lowers climate change, a key concern for this century. Moving away from traditional fossil fuels and toward low-carbon technologies is essential. Since it is a crucial source of clean, low-carbon energy, wind power has significantly contributed to the change in the global energy supply. The worldwide renewables research (Arthouros, 2021) projects that by 2020, wind power capacity will provide more than 6% of total electricity. Offshore wind has expanded significantly during the last ten years. The cumulative offshore installations have grown on average by 22% yearly over the previous ten years, hitting 35 GW in 2020, which is 14 times more than it was ten years ago, according to the Global Wind Report 2021 (GWEC, 2021) published by the Global Wind Energy Council. Over 235 GW of new installations will be finished in the next ten years. Wind energy systems have emerged as a potential technology for harnessing offshore wind resources for large-scale electricity generation since wind power usage is expanding quickly worldwide. Larger OWT systems are being developed and proposed for offshore operations, where the environment is less restrictive [1] due to less ground friction at sea compared to onshore and more space to place larger wind farms.

Using new materials and sustainable construction methods has gained popularity in recent years. Glued laminated timber has become an adaptable and environmentally responsible replacement for conventional building materials. A structurally engineered wood product called glulam comprises layers of solid timber that have been joined using strong adhesives. An introduction to glulam and its use in the building sector is given in this chapter. The earliest applications of laminated wood in Europe occurred around the turn of the 20th century, giving rise to the idea of glulam. However, glulam didn't become well-liked as a building material until the 1930s. The strength and durability of glulam significantly improved during the ensuing decades as a result of developments in adhesive technology and production techniques, broadening its uses.

The sustainability of glulam is one of its main benefits. Compared to other structural materials like steel and concrete, glulam manufacture uses much less energy. Additionally, as wood is a renewable resource, sustainable forestry techniques guarantee that the cut timber will be replaced. Besides, glulam sequesters carbon dioxide, lowering a building's carbon impact. Its application in building encourages a greener strategy and helps facilities earn sustainable building certifications. Numerous different construction styles and structures use glulam. Commercial buildings, hotels, sports facilities, bridges, and even private residences frequently employ it in construction. Due to glulam's adaptability, structures may be designed innovatively, such as with curved beams and intricate geometries, enhancing their visual appeal. Additionally, glulam's small weight makes building and shipping procedures simpler.

1.2. Objective

This thesis aims to design and build a model of an FWTLP using glulam timber to deliver a concept that can compete with steel alternatives.
Wind turbines are being used more often to generate power. Because of the incredible wind speeds, more reliable wind patterns, and less noise and aesthetic consequences for urban areas, offshore wind turbines (OWTs) are a desirable option for energy conversion. Compared to turbines that are on land.

The electrical grid is already connected to some wind turbine installations in shallow water (less than 45 meters), utilizing solid foundations like monopile, gravity, or jacket constructions. Wind turbine support platforms for intermediate water depth (45 - 150 m) and deep water (> 150 m) are also being taken into consideration to exploit a greater wind resource and move the noise and visual impacts farther offshore.
Although fixed jacket structures may be appropriate for some intermediate depths (45 - 80 m), gravity and monopile foundations are not economically viable. Many different floating wind turbine designs have also been proposed, including tension leg, semi-submersible, and spar platforms (HYWIND TAMPEN).

The expense of floating wind turbines (FWT) and the reason they are a relatively new technology are currently limiting factors for FWT designs. Reduced construction and installation costs may result from design advancements and improved load estimates.

Deep-water offshore wind technology has become more widely used in recent years. Installing wind turbines at locations with deeper sea depths, previously impractical for wind energy generation, is now possible thanks to technology. Due to its capacity to produce substantial amounts of renewable energy with little aesthetic and environmental effect, deep sea offshore wind has grown in popularity.

The HYWIND Tampen project, carried out by Equinor [2], a Norwegian energy corporation, is one major project in deep-water offshore wind. Several oil and gas platforms will benefit from the project's installation of floating wind turbines in the North Sea, producing electricity. The platforms will be linked to the turbines via cables that will be moored to the ocean floor. Because it shows the potential of deep-water offshore wind technology in the oil and gas industry, the HYWIND Tampen project is particularly significant. Equinor reduces its carbon footprint and helps the world transition to sustainable energy sources by utilizing renewable energy to power its platforms. The project acts as a proof-of-concept for additional uses of deep-water offshore wind. The HYWIND Tampen project's floating turbines can endure the harsh ocean environment, making them appropriate for installation in locations with deep oceans and strong winds.

In general, expanding deep-water offshore wind technology, as demonstrated by initiatives like HYWIND Tampen, is a positive development for the future of renewable energy. Deep-water offshore wind has the potential to significantly contribute to satisfying global energy demands while reducing environmental effects as the world continues to move toward sustainable energy sources.

1.3. Aim and scope.

This thesis investigates the design and global analysis of a single-column hybrid timber-steel 15 MW TLPWT design with numerous tendons in light of the previously mentioned challenges and similar work in the area. The work aims to provide a concept for sustainable material selection used for offshore applications and an alternative to the existing TLP concepts for OWT.
The design is limited to a single-column TLP with three pontoons with one tendon per pontoon. Further focusing on the structural integrity when using glulam as the primary material.
Global dynamic response both coupled and decoupled is not included in this thesis. For example, the operational coupled behaviour for the turbine and platform is not included. The manufacturing and installation process is not studied. Further, this thesis does not investigate the economic aspects for this concept.

This thesis is divided into nine chapters. Chapter 2 gives the general theoretical background and a relevant literature survey. Chapter 3 provides a more detailed exposition of the underlying theory in the form of the design process used to solve the thesis. Chapter 4 provides a preliminary design. In chapter 5 the results obtained for the previous chapter is shown. Chapter 6 is the results from global analysis with. In chapter 7 the results obtained through this thesis is discussed and in chapter 8 the conclusion is given. In the last chapter further work is listed.

Chapter 2 Theoretical Background

2.1. Literature

2.1.1. Computer programs

In this thesis, a few programs have been used to help solve the main issues. Engineering, business, and science are just a few sectors where computer programs have become indispensable tools. Microsoft Excel and Ansys Workbench are standard computer tools used in these sectors. Spreadsheet software like Microsoft Excel is frequently used for computations, modelling, and data analysis. Engineers and scientists in various sectors favour it because of how simple and versatile it is to use. Numerous mathematical operations, such as statistical analysis, regression analysis, and data visualization, can be carried out in Excel. To aid users in understanding data, it may also be used to produce graphs, charts, and other visual aids.

Ansys Workbench is a simulation program frequently used in research and engineering. Users can utilize computer simulations to model and examine intricate systems and structures. Finite element analysis (FEA), computational fluid dynamics (CFD), and other simulation techniques may be carried out using Workbench. Using these simulations, users may improve designs before creating and forecasting a system's performance under certain circumstances. Workbench and Excel both offer specific benefits and uses. Workbench is more suited for engineering simulations, whereas Excel is better for data analysis and modelling activities. To build more intricate models and simulations, these tools may be combined. For instance, Workbench simulation input data may be created in Excel, and Workbench outputs can be imported into Excel for additional analysis and visualization.

For preliminary design and spreadsheet calculations, Microsoft Excel has been used to calculate the initial geometric input for the model. By following the procedure of [3], the initial length (L), width (W), and height (H) of the TLP leg are calculated.

After getting the initial input, it is then transferred to Ansys Workbench for further processing. Ansys workbench is an FEA program. And by creating a model in this program, it is possible to read the output response for the model and thereby use it to make the final design for the TLP.

To summarise, Microsoft Excel and Ansys Workbench are robust software applications now commonplace in many industries. Excel is the finest modelling and data analysis tool, whereas Workbench excels at engineering simulations. Both systems have advantages, and when combined, they may produce potent tools for tackling challenging issues.

2.1.2. Foundations

There are many types of foundations when discussing different applications for offshore wind turbines. For shallow water (<45m), a fixed jacked may be the most suitable foundation type, and for water (<80m), it may be more economically reasonable with a fixed foundation in comparison with a floating one. But when the water depth increases to (>200m), the fixed foundation becomes too large and expensive compared to a floating foundation. A barge, semi-submersible, spar- or tension-leg platform will be a prevailing option here. These preliminary concepts are considered at this water depth (200m), a semi-submersible with widely spaced columns; a catenary moored spar requires a deep keel and heavy ballast for stability and a TLP design dependent on mooring stiffness for stability. The different foundation types are shown in Figure 1, which illustrates the various drafts and space needed for mooring systems.

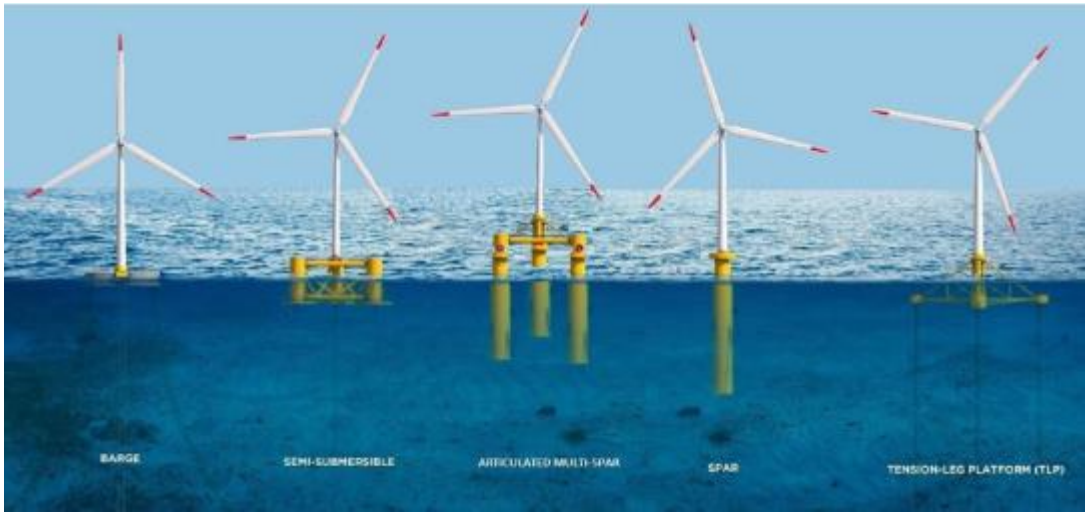

Figure 1: Types of floating foundations.

All these concepts come from the oil and gas industry, each with its beneficial attributes. For wind industry applications, it is essential to note that all concepts depend on the natural frequency. The foundation needs to avoid the ocean wave frequency but also avoid the turbine rotational frequency (especially, the f_{1p} rotor frequency and the f_{3p} frequency).

While a fixed foundation can be described as “soft-stiff” (i.e., the foundational eigenfrequency is between f_{1p} and f_{3p}), when discussing floating foundations, it introduces more complexity because floating foundations such as semi-submersibles and spar-types have three additional degrees of freedom (DOFs) to consider. Here roll, pitch, and surge make a difference and should have a lower frequency than the wave frequency. The tower bending frequency normally lies within the soft-stiff category, as the natural frequency is between f_{1p} and f_{3p}.

The spar-type configuration has a low cost and simple installation compared to the TLPW, and with significant natural stability, it is an attractive concept. Equinor now utilizes them through the Hywind Tampen project [2], a wind park project that will supply Snorre and Gullfaks oilfields with wind energy. This project has a total capacity of 88MW.
Semi-submersible concepts are currently in consideration for both intermediate and deep-water applications. With its three columns and heave plate, it holds excellent stability properties.

One design for consideration is [4–6] Roddier et al.’s design, published in three different papers; the “WindFloat” is a virtual pitch and yaw-free system compatible with any standard offshore turbines; this includes turbines as large as 5MW.
The TLPWT are fundamentally different from the spar- and semi-submersible concepts. Firstly the natural frequencies of the vertical motions (heave, pitch, and roll) of the TLP are placed above the wave frequencies rather than below. Also, the combined tower bending and platform pitch mode of large TLPWTs to the f_{1p} and f_{3p} are considered to be soft-stiff or stiff-stiff, depending on the tendon stiffness and tower design. This concept is promising for use where catenary mooring systems design is challenging, and due to the limited platform motions, the expected structural loading on the tower and blades is reduced.

2.1.3. Previous thesis

MIT was the site of significant early research on TLPWT ideas, including multiple master's and PhD theses.

A 1.5 MW TLPWT in 200 m of water was the subject of a coupled dynamic study in Withee's PhD dissertation (MIT, 2004) [1]. It was not necessary for reliable float-out, unlike other MIT TLPWT designs.

As a result, the design offers approximately 200% reserve buoyancy and has no ballast. According to computational free decay studies, the wind turbine dominates the yaw and pitch damping, but viscous drag is more significant in translational modes of motion. According to operational models, the tower's fatigue life dramatically shortens, and its power production drops by around 1% compared to land-based turbines. Withee concluded that the structural loads resulting from the extreme wind or wave occurrences on the parked turbine would be lower than the operating loads on turbine components due to the functioning of the power take-off system.

Building further on Lee's thesis and Wayman's, Tracy examines the parametric design of single-column support structures for a wind turbine with taut catenary-, tension leg- and catenary mooring systems [7].

Two 1.5 MW TLPWT concept designs were proposed in Lee's master's thesis (MIT, 2005): a spar-type buoy with eight tight tendons at 35-42 and a three-legged floater with vertical tendons [8]. For an uneven sea state with a steady breeze, linear seakeeping evaluations were conducted. The linear damping matrix was expanded to include aerodynamic damping, with the structure being treated as a rigid body. Higher harmonic occurrences were briefly studied, and it was proposed that nonlinear wave excitation may be significant.

WAYMAN et al. initially presented the MIT-NREL TLP for a 5 MW wind turbine in 2006 [9]. Assuming that the tendons had infinite stiffness, rigid body motion was considered; with the wind turbine mounted, the design allows for a stable ballasted tow-out and incorporates about 50% reserve buoyancy when it is in use.

2.2. Glued laminated timber.

2.2.1. Timber

In the recent decade, tremendous technical advances and breakthroughs in the timber construction industry have expanded the range of uses for timber structures in the building industry. For example, timber is now increasingly used for long-span designs. As a result, assessing long-span timber structures has become increasingly important, which has sparked growing interest among professionals in assessment methods for existing timber structures [10].

One of the first offshore oil drilling platforms was built in 1887 off the southern California coast near Santa Barbara. It was merely a wooden dock equipped with a drilling rig for vertical drilling into the seabed. More substantial platforms supported by wooden piers were then built for oil drilling, including platforms for a kilometre-deep well in Caddo Lake, Louisiana (1911), and Lake Maracaibo, Venezuela (1927) [11].

Not long after the construction of these early pier systems, it became clear that attacks by marine organisms drastically reduced the lifespan of wooden structures built in lakes or seas. For this reason, reinforced concrete replaced timber as the load-bearing structure for many offshore platforms by the late 1940s. Over the next 50 years, some 12 000 offshore platforms were built, usually of steel, but more recently of precast concrete.

It is important to remember that wood was also used in shipbuilding. Due to its availability, usefulness and resistance to rotting and decay, wood was a common material. Due to their greater strength and durability, iron and steel, introduced in the 19th century, soon replaced other materials as the preferred choice for shipbuilding.

Since boats and ships have been built, wood has been used in vessels and shipbuilding. Different types of wood are used for creating watercraft in other parts of India. The ruler of Dhar, Bhoja, wrote the Yuktikalpataru (the Wishing Tree of Skill) in the eleventh century AD. It contains a detailed description of boats, ships and the many types of wood used to build them. Although the use of timber for shipbuilding has declined in recent years, some types of ships, small boats and traditional sailing vessels, shown in Figure 2, have renewed interest in the material.

Figure 2: Wooden ship construction.

Due to its natural insulating properties, aesthetics and ease of maintenance, wood is preferred for many purposes. Research and development into the use of wood in larger boats, such as cargo ships and ferries, is continuing to reduce the shipping industry's environmental impact. Wood has a lower carbon footprint than traditional shipbuilding materials such as steel and aluminium, making it a potentially cost-effective alternative in some cases.
However, there are disadvantages to using wood in ships, such as moisture problems, flammability problems and dimensional stability problems. These difficulties need to be addressed when using wood for shipbuilding. With the right design, material selection and maintenance techniques, these problems can be solved. Wood has a long history in shipbuilding but is not widely used today. However, there is renewed interest in using this material in specific ship designs, and future research and development could lead to broader use of wood in larger vessels. Similar to offshore construction, the issues associated with the help of timber in ships need to be appropriately assessed and managed to ensure safe and sustainable operation.

The use of timber in hostile marine environments raises several issues, notwithstanding the effectiveness of timber structures offshore. There are fire resistance issues, flammability and susceptibility to moisture and decomposition. However, these difficulties can be solved with proper design, material selection and maintenance methods. Timber has been used in several offshore construction projects, proving its suitability.

Although timber has long been a popular construction material, the use of timber in offshore projects is a relatively new concept. Nevertheless, timber has become accepted as a suitable material for offshore construction, and there are several examples of timber structures in offshore locations worldwide. One of the main advantages of wood is its remarkable strength-to-weight ratio, which makes it particularly suitable for lightweight components in offshore projects. In addition, wood's renewable properties, sustainability and low carbon footprint make it particularly sought after for projects that promote environmental sustainability.

In 2019, Manik et al. [12] started new research in the glulam field with promising results. Compared to a horizontal arrangement, laminated petung bamboo with a brick arrangement gave the best compressive strength value of $62.68\ MPa$. Even though the value of the brick arrangement is higher than the other, it can be said to be comparable. However, the variations in the laminated apus and petung bamboo structures do not correlate significantly. Compared to a horizontal arrangement, the compressive strength of petung bamboo increased by 8.88% with a brick arrangement, while laminated apus bamboo only increased by 4.77%. According to the BKI, the second class of strength includes the figure for the absolute compressive strength of laminated bamboo. Compared to glulam, with a compressive strength of $30\ MPa$, this could lead to promising results in the application in the building sector.

Despite the difficulties, the use of timber in offshore structures is becoming increasingly popular due to its potential environmental benefits. The future expansion of the use of wood in the offshore industry is hopeful and depends on ongoing research and development in this area.

As the construction industry is one of the most significant users of energy and natural resources, it has a lot to answer for in this regard, according to Lu et al. [13]. It contributes significantly, accounting for one-third of global greenhouse gas emissions, Gan et al. [14], and consuming up to 40% of total energy, Liu et al. [15]. In addition, the sector is responsible for using 12% of available water resources and 3 billion tonnes of natural resources ($40-50\%$ of the total flow in the global economy), Martin and Perry [16]. The renewable status of wood and its low carbon footprint make it a desirable material for offshore projects. Wood

has a lower carbon footprint than traditional materials such as steel and concrete. It is a carbon-neutral substance that efficiently lowers the carbon footprint of offshore structures by absorbing and storing carbon dioxide during its development. Compared to steel and concrete, timber has a lower energy footprint during manufacture and transportation, reducing greenhouse gas emissions. Although using wood in the construction of offshore installations presents challenges in resilience, maintenance and safety, careful consideration of these aspects through appropriate design, material selection, and maintenance approaches ensures safe and long-lasting operation.

Due to its exceptional environmental friendliness, elegance and adaptability, timber is receiving increasing attention as a construction material as the world moves towards a future with limitations on CO2 emissions, according to Gold and Rubik [17]. Wood is derived from trees that rely on solar energy. Like all plants, they release oxygen into the atmosphere and convert CO2 into carbon, according to Newell and Vos [18]. Consequently, it is a material that is renewable, recyclable and biodegradable. It requires little energy to produce and process, and its use in construction helps combat the greenhouse effect, according to Balasbaneh and Bin Marsono [19]. Promoting wood in the construction industry is an important policy objective needed to advance the economy and develop a new paradigm based on biological raw materials and renewable energy, Purkus et al. [20]. According to Bin Marsono and Balasbaneh [21], using wood in the construction industry can contribute to achieving these goals.

2.2.2. Glued laminated timber.

Glulam is a composite material containing wood, glue and, in some cases steel reinforcement. This thesis uses glulam type GL30h, indicating that the adhesive is water-resistant. Glulam is a stress-rated material typically produced with two or more layers of lamstock that are glued together and where the laminations are aligned parallel to the length of the beam [22]. The structure will spend its lifetime in a harsh marine environment, so water- resistance is an important feature. The fundamental properties of GL30h are provided in Table 1. One of the most beneficial mechanical properties of GL30h is the high strength-to-weight ratio. With a density of only $480\ \frac{kg}{m^3}$ compared to steel with a desity of $7800\ \frac{kg}{m^3}$ the weight comparison is quit big. And given its low weight, glulam is one of the strongest construction materials. The high tensile strength of $30\ MPa$ is an important feature when designing a TLP exposed to huge loads. And compression strength of $24\ MPa$ but in a study provided by McConnell et al.

[23], the compressive strength was 1,56 times higher with an STD of 1,9, given by the manufacturer in the material properties for the selected product, with a mean compression strength of 37,5 MPa, which provides a saftynet for this thesis. The study also shows the mean tensile strength obtained was 2,33 times higher than advertised, with a STD of 6,8, which implies a high variability caused by defects inherent in wood.

Table 1:Mechanical properties of GL 30h.

PROPERTY	COMBINED GLULAM	UNIT
STRENGTH CLASS	GL 30h	
STRENGTH CLASS LAMINATIONS	T21, 38	$\frac{N}{mm^2}$
DENSITY	480	$\frac{kg}{m^3}$
DEFLECTION $f_{m,g,k}$	30	MPa
TENSION $f_{t,0,g,k}$	30	MPa
TENSION PARALLEL $f_{t,90,g,k}$	24	MPa
COMPRESSION PARALLEL $f_{c,90,g,k}$	24	MPa
MODULUS OF ELASTICITY $E_{0,g,mean}$	13600	MPa
$E_{0,05}$	11300	MPa
MODULUS OF ELASTICITY PARALLEL $E_{90,g,mean}$	300	MPa
SHEAR MODULUS $G_{g,mean}$	650	MPa

With a higher and higher focus on the environment, glulam is the product that may lead the industry into a new era; due to its zero-emission production, glulam is also recyclable. In the cradle-to-gate life-cycle analysis [22], the hazardous air pollutants released to obtain one cubic meter of glulam is $0{,}34\frac{kg}{m^3}$, which is a low number. And as wood akts like a carbon pool, by withdrawing CO_2 from the surrounding environment the low emission number is

then canceled out and making the wooden product zero emission [24]. Suppose embodied emissions are less than atmospheric carbon stored in the wood product. In that case, the argument that using wood products in the built environment reduces carbon emissions can be supported. The embodied emissions of a product are those associated with its production, such as the CO_2 equivalent emissions from transport, the electricity used for planing and sawing wood products, the CO_2 emissions from the use of gas to heat stoves, etc. According to Pingoud and Lehtilä's study in 2002 [25] on wood products in Finland, processing-related greenhouse gas emissions accounted for only 7% of the CO_2 equivalents contained in sawn wood products.

As a structural member, glulam requires high durability. Okada et al. [26] conclude in their study on glulam durability that even under a high number of cyclic loading after accelerated ageing treatment. The shear strength decreased with increased cycle number but with no change in wooden- failure percentage. It was then assumed that the decrease in shear strength was due to the genesis and development of cracks in the wooden part rather than in the adhesive.

The grains' orientation is shown in Figure 3, and as one can see, the bottom member is flipped 180 degrees. When the wood dries up, it usually bends and twists, but due to the orientation of the grains, it’s dimensionally stable. The direction makes it so that when the wood starts to bend, it bends into the next layer, which bends back, resulting in a standstill and no global or significant local bending or twisting. Glulam is layered wood, and it is formable in almost every form. This makes it possible to obtain prominent cross-section members.

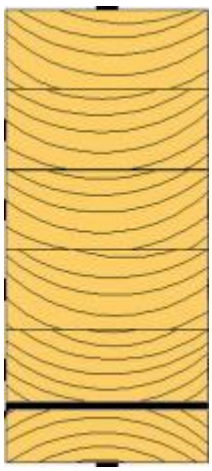

Figure 3: Grain orientation.

2.3. Steel

High-strength, low-alloy (HSLA) structural steel F690W is widely utilized in the building and maritime sectors and has good mechanical qualities. It is renowned for its outstanding toughness, strength, and weldability, making it appropriate for high-strength and impact-resistant solid uses.

F690W steel has a minimum yield strength of $690\ MPa$ [27], shown in Table 2. High strength makes the material excellent for structural components subjected to high loads, such as offshore platforms and shipbuilding, where it can endure significant loads and stresses.
The capacity of F690W steel to withstand fracture under impact loading or abrupt shock is referred to as its toughness. Because of its exceptional durability, it can resist dynamic and demanding situations, including maritime applications where it could run into challenging circumstances like waves and collisions.

F690W steel has strong weldability, enabling it to link structural components quickly and effectively using welding techniques. Arc welding, gas metal arc welding (GMAW), and submerged arc welding (SAW) are all standard welding methods that may be used to join F690W steel. However, as with any steel, suitable welding processes and precautions should be followed to preserve the required material qualities and guarantee weld integrity.
F690W steel has strong corrosion resistance, particularly in maritime situations. It has alloying components that increase its resistance to corrosive media like salt water and the atmosphere. Nevertheless, appropriate surface treatments, such as paint or galvanization, should further protect F690W steel against corrosion.

F690W steel has an impressive level of formability but is mainly utilized for its high strength. It can be twisted and sculpted into many different shapes without losing any of its mechanical qualities. However, compared to steel with lower strength, it may take more energy to create the material because of its higher strength.

Table 2: Mechanical properties for F690W.

STEEL DESIGNATION	**YIELD STRENGTH [MPa]**	**ULTIMATE YIELD STRENGTH [MPa]**
F690W	690	898

Orlov at. al. [28] predicted in their paper that the yield strength for F690W by using selective laser melting (SLM) or using direct laser deposition (DLD) would increase an amount, as shown in Table 3.

Table 3: Mechanical characteristics for specimens from alloy F690W.

TECHNOLOGY	**YIELD STRESS**	**YOUNG'S MODULUS**	**TENSILE STRENGTH**
DLD	823 ± 5	$210{,}7 \pm 2$	971 ± 5
SLM	738 ± 3	218 ± 9	911 ± 2

Based on this information, the confidence in choosing this specific steel grade is heightened.

2.4. Loads on OTLP-WT

This chapter focuses on the different loading on the structure. In the harsh offshore environment, external loading are great, and Figure 4 illustrates the different loadings that is expected in a FOWT. Above SWL wind force acts on the tower and rotor, causing a rotor thrust force. Slamming forces from waves acts on the tower base, and below SWL current acts on the pontoons and on the tendons. Boyancy force act as a counter to the gravitational pull in the global system. Figure 4 also icludes the rotor thrust for IEA 15MW WT, and shows that the maximum thust force is 2,75MN. And the maximum at the end of Region 2 with force equal to 2,75MN. After peaking, the thrust force is reduced due to the increase in blade pitch angle to optimize the generator power of 15MW.

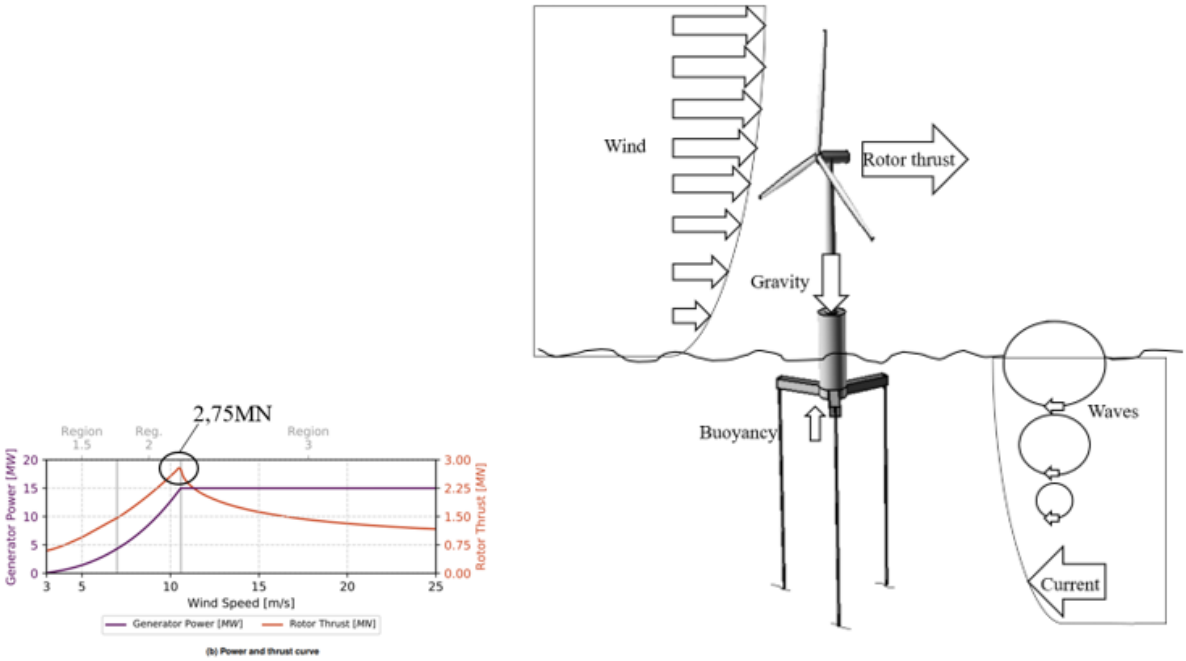

Figure 4: External forces.

Figure 5 illustrates the turbine's different loadings, including hydrostatic pressure, tendon force, and maximum thrust force.

The hydrostatic pressure in the model, illustrated in Figure 5 with letters A, B, C, E, F, G, H, I & J. represents the pressure at 50- and 60m water depth.

The tendon force is applied to pontoons 1 and 2. Due to restrictions in Ansys, a displacement equal to zero in all directions has been added to the end of Pontoon 3. As a result, the tendon

force for pontoon 3 is negligible, and only pontoons 1 and 2 can be used to see the behaviour of the structure. The force is applied directly on the end beams, so the shell does not take the loading.

Also, the turbine's maximum thrust force is added to the centre structure, which is then turned rigid to see the pontoon reaction. The thrust force is applied as a remote force (L), as the thrust force has its centre at rotor height, 170m above the pontoons.

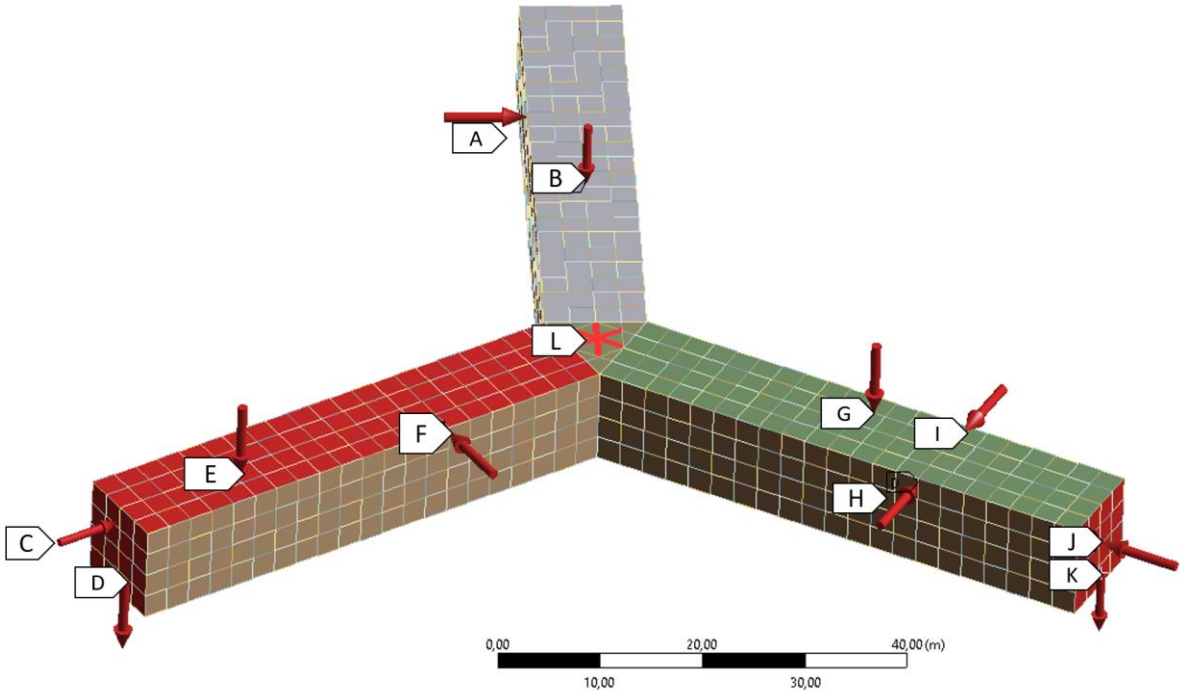

Figure 5: TLP with loading.

Where:

A, B, C, E, F, G, H, I & J	Hydrostatic pressure.
D, K	Tendon force.
L	Thrust force.

2.4.1. Hydrostatic pressure

From DNV-RP- C205 [29], the hydrostatic pressure is calculated for equation (1):

$$\sigma_w = \rho g H \quad (1)$$

Where:

- ρ Water density
- g gravity
- H Hight from SWL

Equation (1) is used to calculate the top and bottom hydrostatic pressure for the pontoons, and for the pontoon's sides, equation (2) is used. Here X indicated the increase in distance from the top of the pontoon towards the bottom. This results in increased pressure applied as a triangular pressure on the structure.

$$\sigma_{w,side} = \sigma_w + \rho g X \quad (2)$$

2.4.2. Tendon force

The tendon force is what holds the TLP in its place. Therefore, Tendon force is the dominating stiffness contribution and a critical load to assess. The assumption that the tendons are straight at all times underlies most estimates of tension leg platform (TLP) surge provided in the literature, which means that transverse deformations of the tendons caused by hydrodynamic and inertial forces may be ignored [30]. The tendon force is discussed more in sub-chapter 0.

2.4.3. Turbine thrust force.

In Figure 4 the ROSCO controller and OpenFAST demonstrate the rotor's steady-state performance as a function of wind speed [31]. Minimum rotor speed restrictions cause higher, unsatisfactory tip speed ratios in regions 1,5. The blade pitch controller sets a minimum pitch limit depending on the estimated wind speed to optimise CP. Low wind speeds lead to positive blade pitch angles of up to 4°. The generator torque controller tries to adjust the rotor to the lowest rotor speed in region 1,5 simultaneously. The torque controller in Region 2 monitors the set point tip-speed ratio, which is set at or close to the maximum CP.

Chapter 3 Design Process

3.1. IEA 15MW

This thesis uses an IEA-15-240-RWT FOWT as a base. Beginning in the early 2000s, the National Renewable Energy Laboratory developed reference wind turbines. The 0.75-, 1.5-, and 3-megawatt (MW) WindPACT turbine series is a product of the National Renewable Energy Laboratory (NREL) [32]. However, they could only be used in national laboratories in the United States. The NREL 5-MW turbine [33], still employed by many academics today, was the first reference turbine broadly embraced by the greater worldwide community. More recently, a 10-MW turbine for offshore wind applications was created at the Technical University of Denmark (DTU) [34]. Other turbines have been added to these two, including a 20-MW conceptual study in the INNWIND project [35], an 8-MW turbine in the European Union FP7 project LEANWIND [36], and studies on 100-meter (m)-blades from Sandia National Laboratories [37]. Most recently, modernized 3.35 MW land-based and 10 MW offshore reference turbines were also made available by IEA Wind Task 37, which oversaw this effort [38]. As the industry quickly increased the power rating and size of its product lines, these designs were released rapidly, one after the other. The average size of a fixed-bottom offshore wind turbine deployed in Europe in 2018 was 6.8 MW [39]. In 2021, GE will introduce its 12-MW Haliade-X offshore turbine with a rotor diameter of 218 m and a direct-drive design.

A new reference wind turbine must advance significantly from the present generation of industrial wind turbines to remain relevant today and in the coming years. Still, it cannot extend to the point where aggressive technological advancements are necessary. The industry and research community's demands too advanced in many areas, including blade scaling, floating foundation design, wind farm control, logistic studies, and other regions, cannot fully satisfy the present collection of reference wind turbine designs. As a result, a reference wind turbine with a unique power and growth trajectory comparable to that of the GE Haliade-X that is over 10 MW but below 20 MW is required.

The Class IB direct-drive IEA 15 MW offshore reference wind turbine has a rotor diameter of 240 meters and a hub height of 150 meters. The second work package of IEA Wind Task 37 on Wind Energy Systems Engineering: Integrated RD&D, NREL, sponsored by the US Department of Energy, and DTU, sponsored by the European Union's H2020 Program, collaborated on the design. Figure 6 describes the aerodynamic performance coefficients for the reference turbine in the three vital zones.

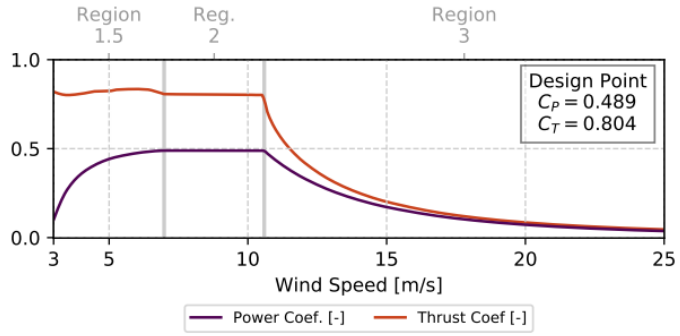

Figure 6:Aerodynamic performance coefficients.

Table 4 describes the properties of the IEA 15MW tower.

Table 4: Tower properties.

PARAMETER	VALUE	UNITS
MASS	1,263	Ton
LENGTH	129,495	m
BASE OUTER DIAMETER	10	m
TOP OUTER DIAMETER	6,5	m
1ST FORE-AFT BENDING MODE	0,496	Hz
1ST SIDE-SIDE BENDING MODE	0,483	Hz

3.2. Design basics

3.2.1. Mechanics of TLP

The interaction between the platform and the surrounding ocean environment constitutes the mechanics of a TLP. The platform is made to stay in one place while floating on the water's surface. The TLP can only move vertically due to the strong connection created by the tendons that attach it to the ocean floor.

The tendons withstand the pressures and transmit them to the platform when waves or currents push on the TLP. The tendons' tension keeps the platform steady and upright by acting as a restoring force.

The TLP's construction enables it to retain stability under challenging oceanic conditions. However, the platform's dynamics are complicated and influenced by several variables. Mentioning a few of these variables are the waves' frequency, shape, and direction. As a result, engineers improve the TLP's architecture for optimum stability using computer simulations and models to forecast how the device would behave under various scenarios.
A TLP's mechanics depend on how the platform interacts with the surrounding ocean environment. The TLP's tendons offer a rigid connection that restricts the platform's mobility to vertical motions. Tension in the tendons, which resists the forces produced by waves and currents, keeps the TLP stable. Optimizing the design through computer simulations ensures the TLP’s stability in all-weather circumstances.

3.2.2. Geometry

A Tension Leg Platform (TLP) 's geometry is crucial in determining its overall performance and functionality. The TLP is a floating offshore platform held in place by tensioned tendons anchored to the seabed, and a range of factors, such as water depth, environmental loads, and operational requirements, influences its geometry. This subchapter will explore the critical aspects of TLP geometry, including the columns' shape and size, the tendons' spacing, and the platform's overall configuration. It will also discuss the factors that must be considered when designing the geometry of the TLP, such as stability, safety, and efficiency. By understanding the importance of TLP geometry and the factors that influence it, designers can create platforms that are optimized for their intended purpose and can withstand the harsh marine environment.

Tension Leg Platforms (TLPs) are typically designed with different shapes and configurations to suit specific environmental conditions and operational requirements. It can affect its stability, efficiency, and overall performance, and it must carefully consider the shape that will best suit the intended purpose of the platform.

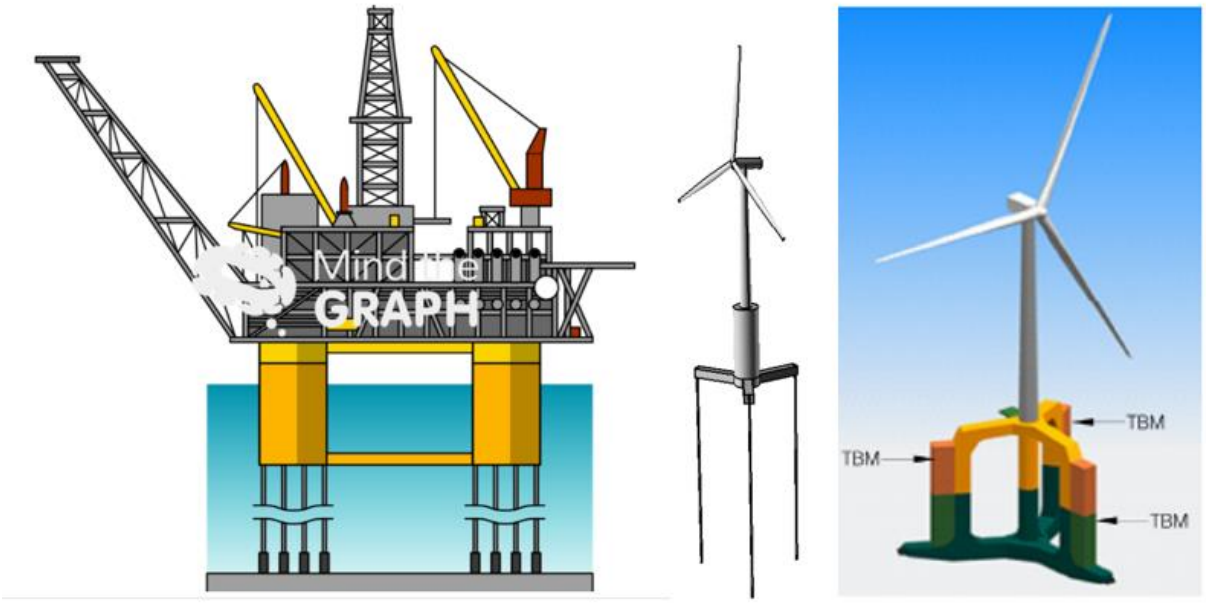

Figure 7: TLP shapes.

One typical TLP shape is the rectangular shape, which consists of four columns arranged in a rectangular pattern, as shown in Figure 7. This shape provides a stable base for the platform and is often used for large-scale offshore oil and gas production and large wind turbines. Another TLP shape is the circular shape, which consists of a single circular column with X legs. The number of legs is decided based on the tendon force required. This shape is highly stable and efficient in low to moderate wave conditions and is often used for small-scale production platforms, such as those used for wind energy. Bachynski [3] developed this concept design with beneficial features exploited in this thesis.

Other TLP shapes, such as triangular and pentagonal, are less common. These shapes are often used for specialized purposes, such as research or exploration. The wind star TLP [40] by Zhao is a unique design compared to the NRELs 5MW concept. The Wind star is smaller and lighter and fits the design requirements set.
GICON has developed a TLP concept, shown in Figure 8. This concept is economical for water depths (>60m). GICONs concepts are for a 2MW and 6MW wind turbine and stretch from 20- 300m water depth.

Figure 8: Gicon- TLP [41].

Overall, the shape of a TLP is an essential consideration in its design and must be carefully chosen based on the platform's specific environmental and operational conditions.

This thesis's selected geometry will be based on the second example, with one central column and three pontoons. The initial pontoon design uses Excel, and then a detailed design will be done using Ansys Mechanical.

Distinctive properties when designing a TLP floater are given in Table 5, and as shown, the surge natural period should be higher than 100 seconds, and the heave period shall be less than 5 seconds.

Table 5: Expected natural periods of deep water floaters [29].

Floater mode	*FPSO*	*Spar*	*TLP*	*Semi*
Surge	> 100	> 100	> 100	> 100
Sway	> 100	> 100	> 100	> 100
Heave	5 – 12	20 – 35	< 5	20 – 50
Roll	5 – 30	50 – 90	< 5	30 – 60
Pitch	5 – 12	50 –90	< 5	30 – 60
Yaw	> 100	> 100	> 100	> 50 – 60

3.3. Design criteria

3.3.1. ULS checklist for global timber model.

Checking the capacity of a notched timber beam [42]:
Firstly, finding the design moment, and the design moment M_{Ed} for a uniformly distributed load is given by equation (4). And then by using equation (5) – (11) to solve for a beam. Further, the rules for larger systems are presented.

Table 6: Modification factor k_{mod} for service classes and load distribution classes [43].

			LOAD DURATION CLASS				
MATERIAL	Associated material standard	Service class	Permanent action	Long term action	Medium term action	Short term action	Instantaneous action
GLULAM	EN 14080	1	0,60	0,70	0,80	0,90	1,10
		2	0,60	0,70	0,80	0,90	1,10
		3	0,50	0,55	0,65	0,70	0,90

The design value of strength properties X_d according to EN 1995-1-1, be calculated as in equation (3). The value of the factor k_{mod} is taken from Table 6, which describes which service class and load duration is to be used. This factor is also used in equation (6) and (9). k_{mod}, which is a modification factor designed to adjust the material properties with respect to load duration but also moisture content. X_k is the materials characteristic strength value, partial factor coefficient (γ_M) for material in ULS is recommended to be equal to 1,25 for glued laminated timber. Wind loading is considered as a short- term load according to Table 6, and because the offshore environment is harsh and very moist, service- class 3 is then chosen. And here $\frac{k_{mod}}{\gamma_m}$ is considered the safety factor.

$$X_d = \frac{k_{mod} X_k}{\gamma_m} \quad (3)$$

$$M_{Ed} = \frac{q_d l^2}{8} \quad (4)$$

The design shear force:

$$V_{Ed} = \frac{q_d l}{2} \quad (5)$$

Then calculate the capacity of the timber element:
Design value for bending strength:

$$f_{m,d} = k_h \left(\frac{k_{mod} f_{m,k}}{\gamma_M} \right) \quad (6)$$

k_h is determined using equation (7):

$$k_h = \min \begin{cases} \left(\frac{600}{h} \right)^{0,1} \\ 1,1 \end{cases} \quad (7)$$

Hereby the bending moment is limited by the following:

$$M_{Rd} = f_{m,d} W \quad (8)$$

And the shear strength:

$$f_{v,d} = \frac{k_{mod} f_{v,k}}{\gamma_M} \quad (9)$$

$$V_{Rd} = \frac{2}{3} A f_{v,d} \quad (10)$$

Because the value for the area A is determined based on the effective width b_{eff}, there has to be added a geometric factor k_{cr}, the equation for shear force capacity is not only equation (10) but now equation (11).

$$V_{Rd} = \frac{2}{3} k_{cr} A f_{v,d} \quad (11)$$

When all the equations above have been solved, it is verified by checking equation (12).

$$M_{Ed} \leq M_{Rd} \quad (12)$$
$$V_{Ed} \leq V_{Rd}$$

According to EN 1995-1-1 [44], the ultimate limit state explains that the required expressions that need to be satisfied are shown in equation (13) when the member is exposed to combined axial tension and bending, and now referred to as design criteria one and two.

$$\frac{\sigma_{t,0,d}}{f_{t,0,d}} + \frac{\sigma_{m,y,d}}{f_{m,y,d}} + k_m \frac{\sigma_{m,z,d}}{f_{m,z,d}} \leq 1 \quad (13)$$

$$\frac{\sigma_{t,0,d}}{f_{t,0,d}} + k_m \frac{\sigma_{m,y,d}}{f_{m,y,d}} + \frac{\sigma_{m,z,d}}{f_{m,z,d}}$$

When subjected to the combination of bending and axial compression, the required expression changes to equation (14) which is design criteria three and four:

$$\left(\frac{\sigma_{c,0,d}}{f_{c,0,d}}\right)^2 + \frac{\sigma_{m,y,d}}{f_{m,y,d}} + k_m \frac{\sigma_{m,z,d}}{f_{m,z,d}} \qquad (14)$$

$$\left(\frac{\sigma_{c,0,d}}{f_{c,0,d}}\right)^2 + k_m \frac{\sigma_{m,y,d}}{f_{m,y,d}} + \frac{\sigma_{m,z,d}}{f_{m,z,d}}$$

Where:

k_m recommended value of 0,70 for rectangular c/s

k_{crit} recommended value of 0,67 for glued laminated timber.

Beam stability due to a combination of bending and compression is considered using equation (15), where a combined moment M_y about the strong axis and compressive stress from N_c occur, the lateral torsional stability must be satisfied. Here $k_{c,z}$ considers the load configuration, the possibility of splitting, and the degree of compressive deformation [45].

$$\left(\frac{\sigma_{m,d}}{k_{crit} f_{m,d}}\right)^2 + \frac{\sigma_{c,0,d}}{k_{c,z} f_{c,0,d}} \leq 1 \qquad (15)$$

Where:

$\sigma_{m,d}$ design bending stress.

$\sigma_{c,0,d}$ design compression stress parallel to the grain.

$f_{m,d}$ design bending strength.

$f_{c,0,d}$ design compressive strength.

k_{crit} reduction factor due to lateral buckling.

$k_{c,z}$ instability factor.

k_{crit} is derived using equation (16), which considers the slenderness of the structure.

$$k_{crit} = \begin{cases} 1 & \lambda_{rel,m} \leq 0.75 \\ 1.56 - 0.75\lambda_{rel,m} & 0.75 \leq \lambda_{rel,m} \leq 1.4 \\ \frac{1}{\lambda_{rel,m}^{\ 2}} & 1.4 \leq \lambda_{rel,m} \end{cases} \quad (16)$$

$\lambda_{rel,m}$, bending relative slenderness and is taken as equation (17):

$$\lambda_{rel,m} = \sqrt{\frac{f_{m,k}}{\sigma_{crit,m}}} \quad (17)$$

$\sigma_{crit,m}$ is the critical bending stress according to the stability theory, and by using a five-percentile stiffness value, the bending stress is derived in equation (18):

$$\sigma_{crit,m} = \frac{0{,}78b^2}{hl_{eff}} E_{0,05} \quad (18)$$

Where:

b	beam width
h	beam hight
l_{eff}	effective length
$E_{0,05}$	fifth- percentile value of the modulus of elasticity.

Effective length (l_{eff}) is dependent on the support type provided by the system. The length ratio $\frac{l_{eff}}{l}$ is given in Table 7. The length ratio between l_{eff} and the span (l) is only valid provided that the beam has torsional restrained support and the load is distributed directly on the COG of the shaft. For beams where the load is applied at the compression edge, the

effective length should be increased by $2h$ and if the loading is used on the tension edge, l_{eff} should be decreased by $0{,}5h$.

Table 7: Length ratio [45].

BEAM TYPE	LOADING TYPE	$\frac{l_{eff}}{l}$
SIMPLY SUPPORTED	Constant moment	1,0
	Uniformly distributed load	0,9
	Concentrated force at the middle of the span	0,8
CANTILEVER	Uniformly distributed load	0,5
	Concentrated force at the free end	0,8

Instability factor $k_{c,z}$ is derived using equation (19):

$$k_{c,z} = \frac{1}{k_z + \sqrt{k_z^2 - \lambda_{rel,z}^2}} \quad (19)$$

And using equation (20) to find k_z:

$$k_z = 0{,}5\left(1 + \beta_c\left(\lambda_{rel,z} - 0{,}3\right) + \lambda_{rel,z}^2\right) \quad (20)$$

For glued laminated timber, β_c is set to 0,1. The slenderness ratio (λ_z) and the relative slenderness ratio corresponding to the bending ($\lambda_{rel,z}$) should be calculated using equations (21) and (22); R is the radius of gyration.

$$\lambda_z = \frac{l_{eff}}{R} \quad (21)$$

$$\lambda_{rel,z} = \frac{\lambda_z}{\pi}\sqrt{\frac{f_{c,0,k}}{E_{0,01}}} \quad (22)$$

3.3.2. Stress analysis in glulam beam cross-section.

Bending stresses in the outer fibres of each component i are determined from an external moment M given in equation (23)

$$\sigma_{i,m} = \frac{M}{EI_{ef}} * E_i * \frac{h_i}{2} \quad (23)$$

The reinforcement of beams notched on the same side as the support is designed for a particular tensile force, known as $F_{t,90,d}$. This tensile force is perpendicular to the grain, corresponding to the tensile stress perpendicular to the grain of the area described in Figure 9 as one. This tensile force can therefore be transferred by glued-in rods, glued-on reinforcement plates, or fully threaded screws.

The first step is calculating the tensile component perpendicular to the grain generated from the external load in critical area 1 according to Figure 9, and this is done by equation (24):

$$F_{t,90,d} = 1{,}3V_d * \eta \quad (24)$$

Because the stresses in the notch corners are not uniformly distributed, which will give peak stresses, the increasing distance from the notched corner must be taken care of by introducing the increase of 30% in equation (24).

Where η is the factor for the joints loaded perpendicular to the grain if α is replaced by $\frac{a}{h} = h_{ef}$ and the term is converted, as shown in equation (25):

$$\eta = 1 - 3\left(\frac{a}{h}\right)^2 + 2\left(\frac{a}{h}\right)^3 \quad (25)$$

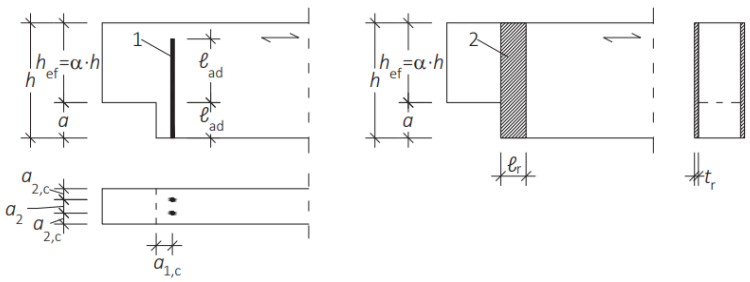

Figure 9: Reinforcement of notched beams with geometric details, 1: Reinforcement with fully threaded screw/ glued-in rod, 2: Reinforcement with glued-on plates [46].

When using glued-in rods, the bond line has to be checked, and now uniform load distribution is assumed when using equation (26):

$$\tau_{ef,d} \leq f_{k1,d} \; with \; \tau_{ef,d} = \frac{F_{t,90,d}}{n d_r \pi l_{ad}} \qquad (26)$$

Table 8 includes the values for $f_{k1,d}$ under different lengths of l_{ad}.

Table 8: Characteristic bond line strength in reinforcement, DIN EN 1995-1-1.

	CHARACTERISTIC STRENGTH $\left[\frac{N}{mm^2}\right]$	**EFFECTIVE LENGTH** ≤ 250	$250 \leq l_{ad} \leq 500$	$500 \leq l_{ad} \leq 1000$
THE BOND LINE BETWEEN THE ROD AND BOREHOLE WALL	$f_{k1,d}$	4	$5{,}25 - 0{,}005 l_{ad}$	$3{,}5 - 0{,}0015 l_{ad}$

3.3.3. C/S subjected to combined stress

Lateral torsional stability should be verified in two different cases: when only considering the bending moment around the dominating axis (M_y) and a combination of the bending moment (M_y) and the compressive force (N_c).

Firstly, the relative slenderness for bending is considered as in the equation according to E1995-1-1 Eurocode 5:

$$\lambda_{rel,m} = \sqrt{\frac{f_{m,k}}{\sigma_{m,crit}}} \quad (27)$$

Here, $\sigma_{m,crit}$ is the critical bending stress according to the theory of stability, using a 5-percentile stiffness value and $f_{m,k}$ is the characteristic bending strength.

Secondly, the critical bending stress is given by equation (28):

$$\sigma_{m,crit} = \frac{M_{y,crit}}{W_y} = \frac{\pi\sqrt{E_{0,05} I_z G_{0,05} I_{tor}}}{l_{ef} W_y} \quad (28)$$

Where:

$E_{0,05}$	fifth percentile value of the elastic modulus parallel to the grain;
I_z	second area moment about the weak axis z;
$G_{0,05}$	fifth percentile value of the shear modulus parallel to the grain;
I_{tor}	torsional area moment
l_{ef}	effective beam length, depending on the support conditions and the load configurations.
W_y	section modulus about the strong axis y.

As this thesis only considers rectangular cross-sections $\sigma_{m,crit}$ can be taken as equation (29) shows:

$$\sigma_{m,crit} = \frac{0{,}78b^2}{hl_{ef}} E_{0,05} \quad (29)$$

And here, b represent the width of the beam's c/s, and h is the height of the beam's c/s.
Then finally, calculating for both cases. Case one with only moment (M_y) should satisfy the expression (30):

$$\sigma_{m,d} \leq k_{crit} f_{m,d} \qquad (30)$$

Where:

$\sigma_{m,d}$	design bending stress
k_{crit}	factor that takes the reduced bending strength into account due to lateral buckling
$f_{m,d}$	design bending strength

Since the beams in the TLP's leg are exposed to torsional bending due to the thrust force from the turbine, the factor k_{crit} is determined by (31):

$$k_{crit} = \begin{cases} 1 & for \lambda_{rel,m} \leq 0{,}75 \\ 1{,}56 - 0{,}75\lambda_{rel,m} & for\ 0{,}75 \leq \lambda_{relm} < 1{,}4 \\ \dfrac{1}{\lambda_{relm}^2} & for\ 1{,}4 \leq \lambda_{relm} \end{cases} \qquad (31)$$

3.3.4. ULS checklist for steel

This subchapter explains the rules and regulations for ultimate limit state design for steel construction; this relates to the waterproof plating for the pontoons of the TLP.

3.3.4.1. Plate without longitudinal stiffeners

For internal elements, Table 9 is used to determine the effective areas of flat compression elements. The following equation (32) should be used to determine the effective size ($A_{s,eff}$) of the compression zone of a plate with the gross cross-sectional area A_s:

Table 9: Internal compression elements [47].

Stress distribution (compression positive)	Effective width b_{eff}
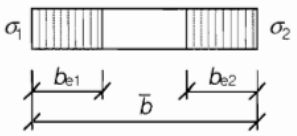	$\psi = 1$: $b_{eff} = \rho\ \bar{b}$ $b_{e1} = 0{,}5\ b_{eff}$ $b_{e2} = 0{,}5\ b_{eff}$
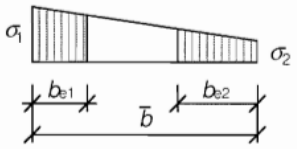	$1 > \psi \geq 0$: $b_{eff} = \rho\ \bar{b}$ $b_{e1} = \frac{2}{5-\psi} b_{eff}$ $b_{e2} = b_{eff} - b_{e1}$
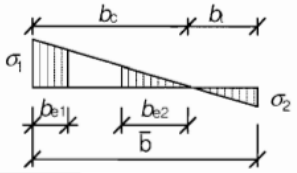	$\psi < 0$: $b_{eff} = \rho\ b_c = \rho\ \bar{b} / (1-\psi)$ $b_{e1} = 0{,}4\ b_{eff}$ $b_{e2} = 0{,}6\ b_{eff}$

$\psi = \sigma_2/\sigma_1$	1	$1 > \psi > 0$	0	$0 > \psi > -1$	-1	$-1 > \psi \geq -3$
Buckling factor k_σ	4,0	$8{,}2 / (1{,}05 + \psi)$	7,81	$7{,}81 - 6{,}29\psi + 9{,}78\psi^2$	23,9	$5{,}98\ (1 - \psi)^2$

$$A_{s,eff} = \rho_{red} A_s \qquad (32)$$

Where ρ_{red} is the reduction factor for plate buckling. The reduction factor can, according to equation (33), be taken as follows:

$$\rho_{red} = \begin{cases} 1 & for \lambda_p \leq 0{,}673 \\ \dfrac{\lambda_p - 0{,}055(3+\psi)}{\lambda_p^2} \leq 1 & for\ \lambda_p > 0{,}673 \end{cases} \quad (33)$$

And λ_p is determined using equation (34):

$$\lambda_p = \sqrt{\frac{f_y}{\sigma_{cr}}} = \frac{\frac{b}{t}}{28{,}4\varepsilon\sqrt{k_\sigma}} \quad (34)$$

Where:

b appropriate width taken from table 5.2 of EN 1993-1-1 [48].

t plate thickness

ψ stress ratio determined in accordance with “4.4(3) and 4.4(4)” [49].

ε $= \sqrt{\dfrac{235}{f_y}}$

k_σ Buckling factor corresponding to the stress ratio ψ and boundary conditions [49].

As there are no transverse stiffeners between the flat plate elements, the plate buckling could be column-like and therefore require a reduction factor ρ_c close to the value of X_c as in the column buckling shown in Figure 10. Also, for the end of the pontoon, where $\frac{a}{b} \geq 1$ the buckling behaviour would have a small aspect ratio α as in Figure 10:

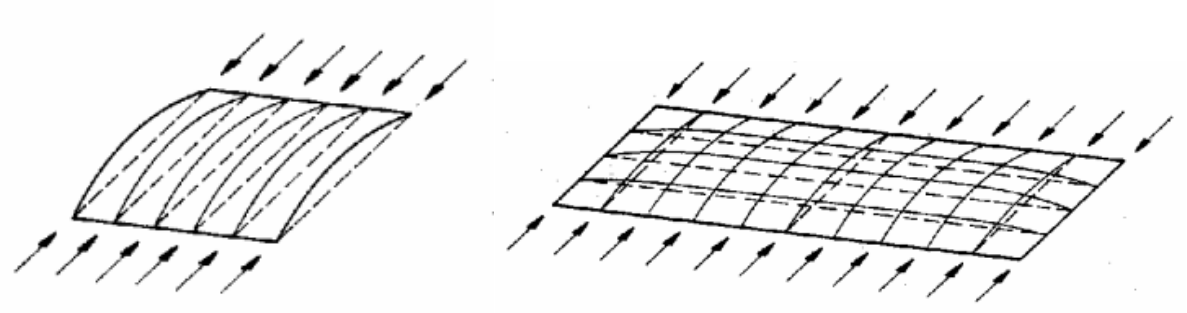

Figure 10: Column-like behaviour with small ratio α [49]

And because the plate is considered unstiffened, the elastic critical column buckling stress $\sigma_{cr,c}$ shall be taken as the buckling stress with the longitudinal edges removed and $\sigma_{cr,c}$ is taken using equation (35).

$$\sigma_{cr,c} = \frac{\pi^2 E t^2}{12(1-v^2)a^2} \quad (35)$$

The relative slenderness of the "column" λ_c is expressed by using the following equation (36):

$$\lambda_c = \sqrt{\frac{f_y}{\sigma_{cr,c}}} \quad (36)$$

3.3.4.2. Interaction between plate and column buckling.

Reduction factor X_c is obtained from 6.3.1.2 of EN 1993-1-1 [48], and because the plate is considered unstiffened $\alpha = 0{,}21$ and corresponding to buckling curve "a", this buckling curve should then be used. Finally, the reduction factor ρ_c can be interpolated between X_c and ρ_s and obtained using equation (37).

$$\rho_c = (\rho - X_c)\zeta(2 - \zeta) + X_c \qquad (37)$$

Where:

ζ $= \frac{\sigma_{cr,p}}{\sigma_{cr,c}} - 1 \quad with\ 0 \leq \zeta < 1$

$\sigma_{cr,p}$ Elastic critical plate buckling stress.

$\sigma_{cr,c}$ Elastic critical column buckling stress.

X_c Reduction factor due to column buckling.

ρ Reduction factor due to plate buckling.

3.3.4.3. Verification

The final part of this chapter includes the verification of plate buckling. Members subjected to compression and biaxial bending should be verified using the following equation (38).

$$\eta_1 = \frac{N_{Ed}}{\frac{f_y A_{eff}}{\gamma_{M0}}} + \frac{M_{y,Ed} + N_{Ed} e_{y,N}}{\frac{f_y W_{y,eff}}{\gamma_{M0}}} + \frac{M_{z,Ed} + N_{Ed} e_{z,N}}{\frac{f_y W_{z,eff}}{\gamma_{M0}}} \quad (38)$$

Where:

A_{eff}	effective cross-section area.
$e_{y,N}, e_{z,N}$	shift in the position of the neutral axis, the eccentricities with respect to the neutral axis.
N_{Ed}	design axial force.
$M_{y,Ed}, M_{z,Ed}$	design bending moment for $y-y$ and $z-z$ axis.
$W_{y,eff}, W_{z,eff}$	effective elastic section modulus for its axis.
γ_{M0}	partial factor [50].

The plate buckling verification should be carried out for the resultant stress at the smallest distance of $0{,}4a$ or $0{,}5b$. This is where the stresses are the greatest, and for this case, the gross sectional resistance needs to be checked at the end of the plate.

Chapter 4 Preliminary design

The preliminary design of a Tension Leg Platform (TLP) is a critical stage in developing a successful offshore platform. The TLP is a floating platform held in place by tensioned tendons anchored to the seabed and commonly used for deep-water oil and gas production. The preliminary design stage involves determining the size, shape, and configuration of the TLP, selecting appropriate materials, and designing the mooring and tendon systems. The design must consider various factors, such as water depth, environmental loads, and operational requirements, and must be optimized to ensure safety, stability, and efficiency. The preliminary design is the foundation upon which the detailed engineering, fabrication, and installation of the TLP are based and is crucial to the success of the entire project.

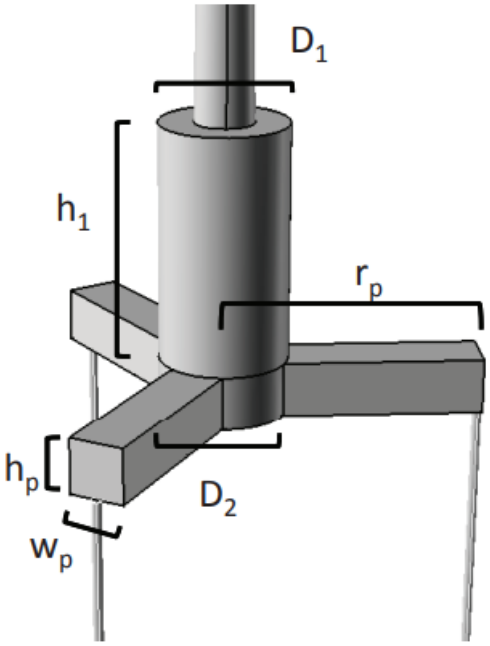

Figure 11: Parametric design description [3].

4.1. Spreadsheet calculation

4.1.1. Added mass estimation.

A rough estimation of added mass requires neglecting some components of the added mass. In this chapter, neglecting the interactions between members and the end effects of any component and 2D added mass coefficients can be applied to each component. For the centre cylinder with a diameter D, the transverse added mass per unit length, a_t is given by equation (39).

$$a_t[D] = \frac{\rho \pi D^2}{4} \quad (39)$$

For a square section with side length h, equation (40) can be applied:

$$a_t[h] = 4.754\rho \left(\frac{h}{2}\right)^2 \quad (40)$$

Then, in equation (41), the summation of the added mass contributions from the pontoons and the central column in the surge is given. The contribution from the pontoons is summed based on the angle around the z axis, with the angle θ. Notice that the length of the pontoons (l_p) is the measured length from r_p to the diameter of the nodal cylinder at the vertical level of the pontoons.

$$A_{11} \approx a_t[D_1](h_1 - b_t) + a_t[D_2]h_2 + \sum_{i=1}^{n_p} l_p a_t\left[h_p\right] \cos^2 \theta_i \quad (41)$$

The added mass in heave is estimated in equation (42) and includes a contribution from the central column given by [3] an approximation that the added mass of the central column can be found by assuming that it has the added mass of a sphere with a diameter of D_2. This diameter is equivalent to the displaced mass of half a sphere with a diameter D_2. Then the contribution of the pontoons is added.

$$A_{33} \approx \frac{\rho\pi}{12} D_2^3 + \sum_{i=1}^{n_p} l_p a_t[w_p] \tag{42}$$

When computing the added mass in pitch and the coupled surge-pitch added mass, the sectional added masses are integrated in equations (43) and (44).

$$A_{51} \approx -\frac{1}{2}(h_1 - b_t)^2 a_t[D_1] - \frac{1}{2}(T^2 - (-T + h_2)^2) a_t[D_2] + \sum_{i=1}^{n_p} \sin^2\theta_i z_s \left(r_p - \frac{D_2}{2}\right) a_t[h_p] \tag{43}$$

$$A_{55} \approx a_t[D_1](h_1 - b_t)\left(\frac{1}{12}(h_1 - b_t)^2 + \left(\frac{1}{2}(h_1 - b_t)\right)\right) + a_t[D_2]h_2)(\frac{1}{12}h_2^2 + \left(\frac{1}{2}(-2T + h_2)\right)^2) + \sum_{i=1}^{n_p} \cos^2\theta_i \left(\frac{1}{3}(r_p^3 - D_2^3) a_t[w_p]\right) + \sum_{i=1}^{n_p} \sin^2\theta_i z_s \left(r_p - \frac{D_2}{2}\right) a_t[h_p] \tag{44}$$

Finally, computing the added mass in yaw. It's done by summing the integrated effects of the pontoons shown in equation (45). Since there is no contribution from the centre column, it's not included in the equation.

$$A_{66} \approx \sum_{i=1}^{n_p} \frac{a_t[w_p]}{3}\left(l_p^3 - \frac{D_2^3}{2}\right) \quad (45)$$

4.1.2. Stiffness estimation

The stiffness comes from the mooring system, with its stiffness matrix due to n_t lines at a position θ_j is approximated, assuming the lines remain straight. When the TLP is in an operational steady state, the thrust force on the turbine causes a horizontal displacement on the structure. Here the tendon force counteracts as a restoring force. The fairlead position is therefore moved from the rest position, which is located directly above the anchor point of each tendon.

When not assuming the tendon does not increase in length due to stretching, theoretically, this horizontal displacement causes "set down". Set down, which is a vertical displacement due to the surge motion. For small surge displacements, a valid assumption is that the length dues do not increase and can therefore be considered constant. By this assumption, the tendon force is also regarded as continuous. Then by applying a small angle approximation and neglecting the tendon mass, the restoring stiffness in surge and sway can be expressed by the following equation (47).

And under an external force in heave, the tendon extends and contracts. The stiffness provided form the tendons is so large that the hydrostatic stiffness is neglectable. However, the complete stiffness in heave can be found using equation (48).

The following equations give the system stiffness:

$$k_{11} = \frac{F_t}{l_0}\,, \qquad k_{33} = \frac{E_t A_t}{l_0} \quad (46)$$

Surge:

$$K_{11} \approx \sum_{j=1}^{n_t} k_{11} \tag{47}$$

Heave:

$$K_{33} \approx \sum_{j=1}^{n_t} k_{33} \tag{48}$$

Coupled:

$$K_{51} = K_{15} \approx \sum_{j=1}^{n_l} k_{11} z_s \tag{49}$$

Pitch:

$$K_{55} \approx \sum_{j=1}^{n_l} \left[k_{11} z_s^2 + k_{33} r_p^2\right] \cos^2 \theta_j \tag{50}$$

Yaw:

$$K_{66} \approx \sum_{j=1}^{n_l} k_{11} r_p^2 \tag{51}$$

Symmetric systems:

$$K_{22} = K_{11} \tag{52}$$

$$K_{24} = K_{42} = -K_{51} \tag{53}$$

$$K_{44} = K_{55} \tag{54}$$

The displacement can then be obtained in the surge direction by taking the thrust force and dividing it by the stiffness K_{11} as shown in equation (55):

$$\eta_1 = \frac{T}{K_{11}} \tag{55}$$

4.1.3. Tendon design

Tendons are an essential component in the design of a TLPWT. They provide additional support and stability to the structure, particularly against the effects of wind, waves, and other environmental loads. The design of tendons requires careful consideration of various factors, including the materials used, the dimensions of the tendon, the load capacity required, and the structure's intended use.

Moreover, the design process must ensure the tendon can withstand the anticipated loads and deformations over its intended lifespan. Therefore, the design of tendons requires specialized expertise and experience in structural engineering and materials science. This segment will delve into the key considerations involved in the design of tendons for the TLPWT.
To keep the varying parameter number as small as possible, the number of tendons n_t will be equal to the number of pontoons n_p.

The tendon area (A_t) must be sufficient to prevent the reach of the yield stress (σ_y), and because this is a preliminary design, the safety factor is chosen to be conservatively high ($SF = 2$) for tensions up to twice the initial tension (F_t) shown in equation (56). Table 10 shows the mechanical properties of each tendon.

$$\frac{F_{pre}}{A_t} \leq \frac{\sigma_y}{SF} \quad (56)$$

Table 10: Tendon mechanical properties.

PARAMETER	SYMBOL		UNIT
DENSITY	ρ_t	7850	$\frac{kg}{m^3}$
YIELD STRENGTH	σ_y	250	MPa
TENDON THICKNESS	t_t	$\approx 0.033 d_t$	mm
UNSTRETCHED LENGTH	l_0		m
TENDON AREA	A_t	$\frac{\pi(D_{to}^2 - D_{ti}^2)}{4}$	mm^2
ELASTIC MODULUS	E_t	$2.11\ x\ 10^{11}$	Pa

The individual pretension for each tendon is calculated by equation (57):

$$F_{pre} = \frac{F_B - F_t}{n_t} \quad (57)$$

Where:

$F_B = \rho g \nabla$

$F_t = m_{tot} g$

And ∇ is the submerged volume calculated from equation (58):

$$\nabla = \frac{\pi}{4}(D_1^2(H_1 - b_t) + D_2^2 H_2) + w_p h_p l_p n_p \quad (58)$$

4.1.4. Scale factor

Scale factor based on natural period, calculated from tendon stiffness.
Based on the calculations from *"Generic Upscaling Methodology of a Floating Offshore Wind Turbine"* [51] upscaling based on column radius gives a conservative result and, therefore, the safest choice when changing the material.
A scaling factor must be applied to various design parameters to increase the wind turbine's capacity from 5 MW to 15 MW. The scaling factor is determined by equating the power output of the full-scale turbine (15 MW) to the scaled model's (5 MW) power output raised to a specific exponent. Depending on the scaled design parameters, this exponent is typically between two and three.

The rotor diameter of the scaled turbine would need to be s_r times larger than the rotor diameter of the full-scale turbine to achieve the same power output per unit area of the rotor. Similarly, other design parameters such as blade length, tower height, and generator size would also need to be scaled up by the same factor to maintain the same power output per unit area of the rotor.

It is important to note that scaling up a wind turbine design has limitations and careful consideration of structural integrity and weight factors. Thus, the design must be optimized to ensure increased capacity without compromising the turbine's safety and reliability.

4.1.5. Natural period and frequency

The surge and sway natural periods should be longer than 25 seconds to avoid wave-excitation. The decoupled natural period T_{n1} is given in equation (59):

$$T_{n1} = 2\pi \sqrt{\frac{M_{11} + A_{11}}{K_{11}}} \quad (59)$$

The heave, roll/ bending, and pitch/ bending natural period T_{n3}should be shorter than 3,5 seconds to avoid the first-order wave excitations as given in the equation (60):

$$T_{n3} = 2\pi \sqrt{\frac{M_{33} + A_{33}}{C_{33} + K_{33}}} \quad (60)$$

Surge and sway natural frequency is shown in equation (61)

$$f_1 = \frac{2\pi}{T_{n1}} \quad (61)$$

And for heave/ bending and pitch/ bending natural frequency f_3, given in equation (62):

$$f_3 = \frac{2\pi}{T_{n3}} \quad (62)$$

4.1.6. Towing

TLP FOWT that is vertically towed out to the installation site, the shape and size of the floater have to be adjusted so that an adequate pitch restoring moment is achieved during towing conditions; this is before the tendons are connected. The steady-state pitch angle is set to 10 degrees [52], and the minimum hydrostatic stiffness coefficient $K_{55,HI,min}$ can be obtained using equation (63):

$$K_{55,HI,min} = \frac{F_5}{\eta_5} \quad (63)$$

Where:

F_5 pitch moment;

η_5 displacement.

Because it will be bigger than the maximum thrust during towing, the pitch moment F5 is calculated using the minimum thrust force during wind turbine operation. By regulating the draft, cylinder radius, and ballast, for which the correlation to hydrostatic restoring in pitch for a cylinder, the necessary restoring is obtained using equation (64):

$$K_{55,HI} = F_B Z_B - (M_{tot} + M_w) g Z_g + \frac{\rho g \pi r^4}{4} \quad (64)$$

4.1.7. Installation

The reserve buoyancy determined by equation (65), which for a towed FOWT is the weight of the water ballast used for stability during towing of the mounted structure, is equal to the tendon pretension. The tendons are attached and pretensioned at the installation location during the removal of the water ballast. Although the centre of gravity will move upward during installation, there won't be any vertical displacement.

$$RB = F_B - M_{tot} g = M_w g \quad (65)$$

4.1.8. Operational condition

Under steady-state operating conditions, the TLP will have a steady-state displacement due to the thrust force on the wind turbine. It is appropriate to assume that the tendons are endlessly rigid to make the computation easier for the static design phase.
The steady-state displacement will be constrained to surge mode due to the TLP being upright. Wayman [9] recommends that the tendons' angle with the vertical plane not be more than 5 degrees, and the associated maximum surge displacement is utilized as a starting point for the tendon tension. Equation (66) may be used to derive the minimal tendon restoring coefficient in the surge, where $F_{thrust,max}$ is the operational maximum thrust force.

$$K_{11,T,min} = \frac{F_{thrust,max}}{\eta_1} \quad (66)$$

The maximum permissible strain for the tendon must not be exceeded during operation, and none of the lines must be slack. Since the three tendons are at a 60-degree angle, all are of equal importance, and when the full thrust force at a zero-degree angle for t_1 (tendon 1), t_2 and t_3 shall not exceed maximum strain.

4.2. Pontoon design

The pontoon features a steel-plated shell of 50mm, as in Figure 12, that covers the inner wooden structure. The shell protects the system from water damage with no intention of carrying heavy loading.

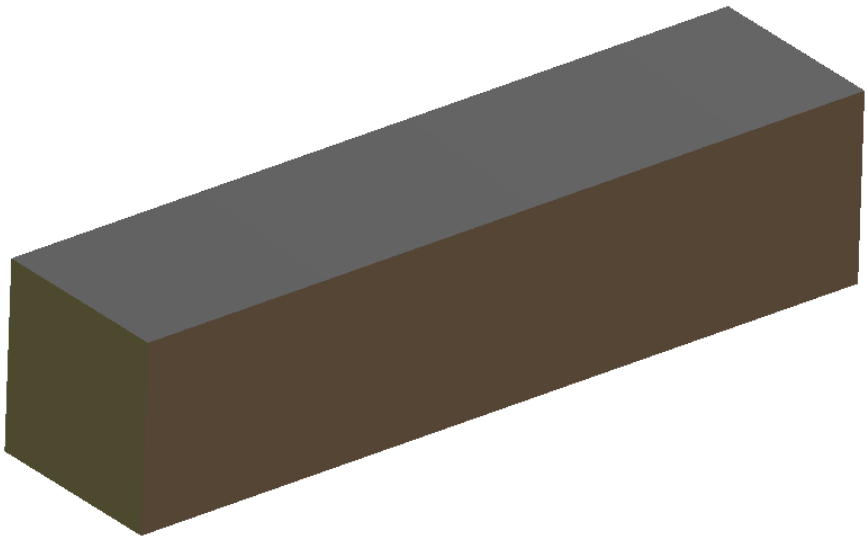

Figure 12: Pontoon with shell.

The cross-section used in this thesis contains two different dimensions. For simplicity, both cross-sections are solid squares, and in Table 11, the dimensions for the given cross-sections are illustrated in Figure 13.

Table 11: Cross-section values.

SYMBOL	VALUE	UNIT
W1	0,75	m
W2	1	m
H1	0,75	m
H2	1	m

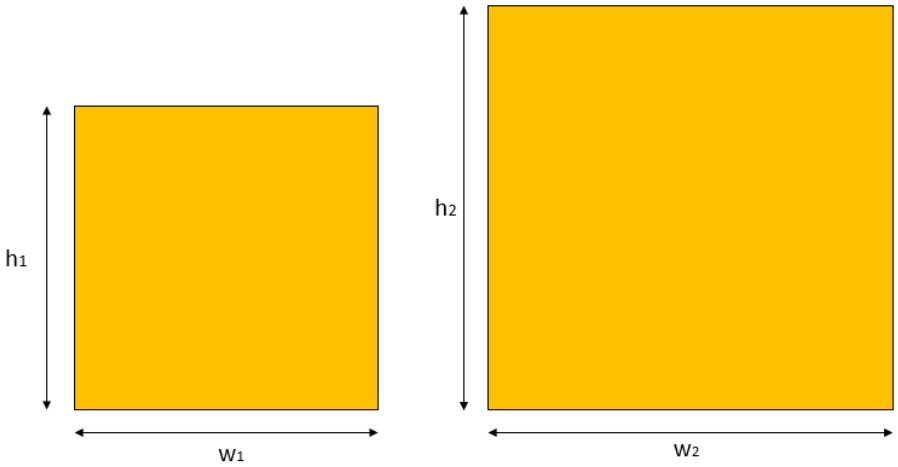

Figure 13: Cross-sections.

Figure 14 shows the pontoon timber structure built symmetrically along the x- and y-axis. For extra reinforcement in the centre, two additional rows of columns have been added, with cc 2500mm. All members are considered beams; the standard cross-section used is 750 x 750mm, and the beams have been enlarged to 1000 x 1000mm due to high stresses in the centre structure. The total height of the pontoon is 10m, its width is 10m, and its length is 52,5m.

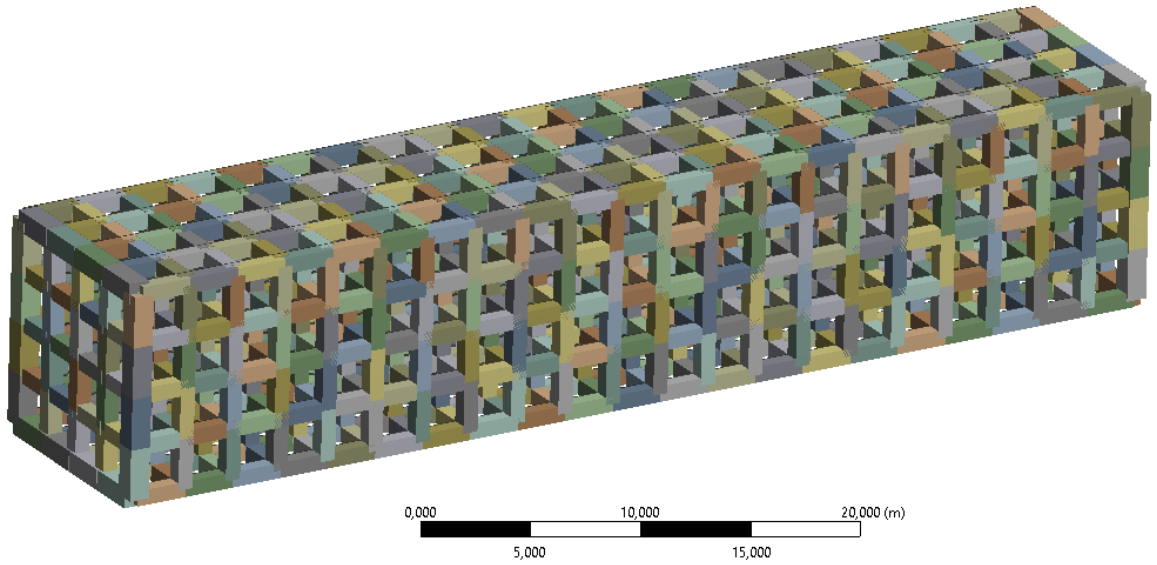

Figure 14:Pontoon timber structure.

4.3. TLP design

The final design for the TLP is illustrated in Figure 15, Figure 16 and Figure 17. Figure 15 shows the shell structure made to keep moisture away from the load-bearing wooden frame shown in Figure 16.

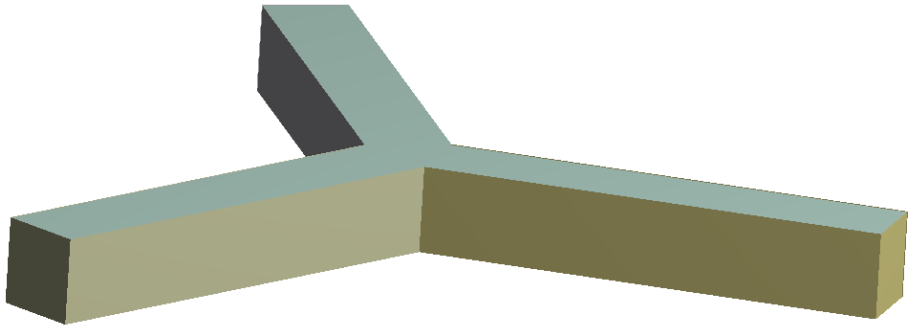

Figure 15: TLP with shell.

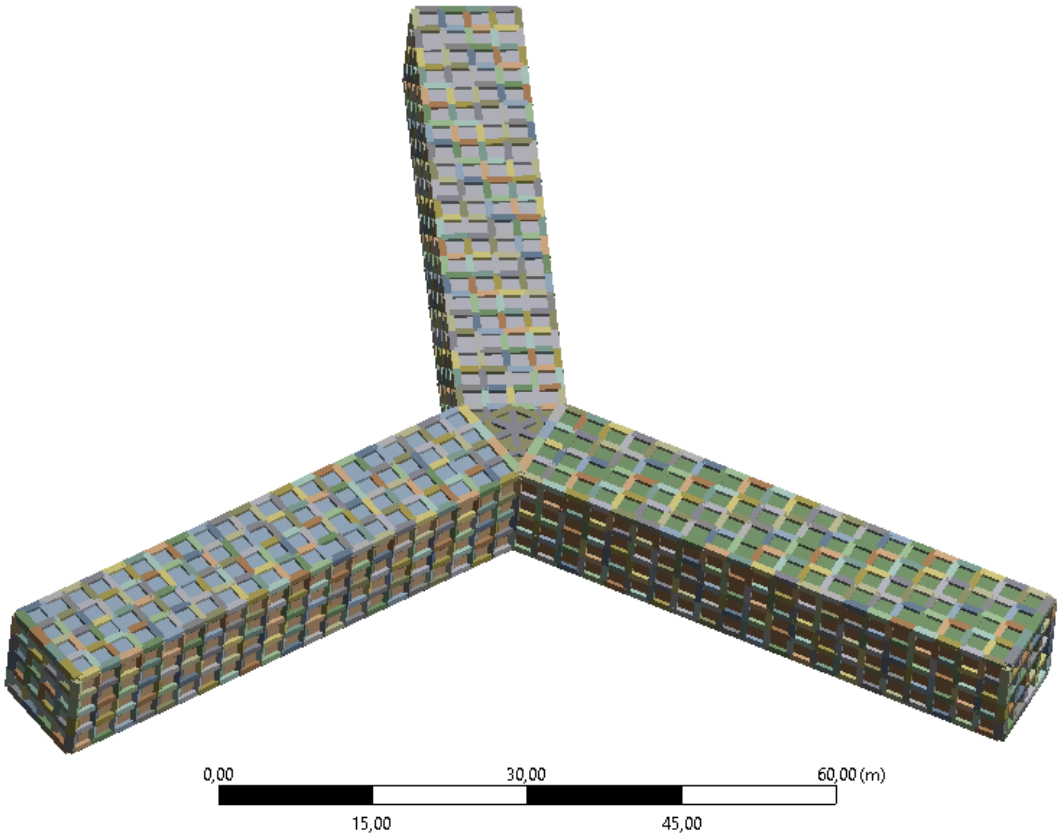

Figure 16:Loadbearing system.

Illustrating the centre construction, it's a hexagon and, as a result of this, transferring the loads from pontoon to pontoon.

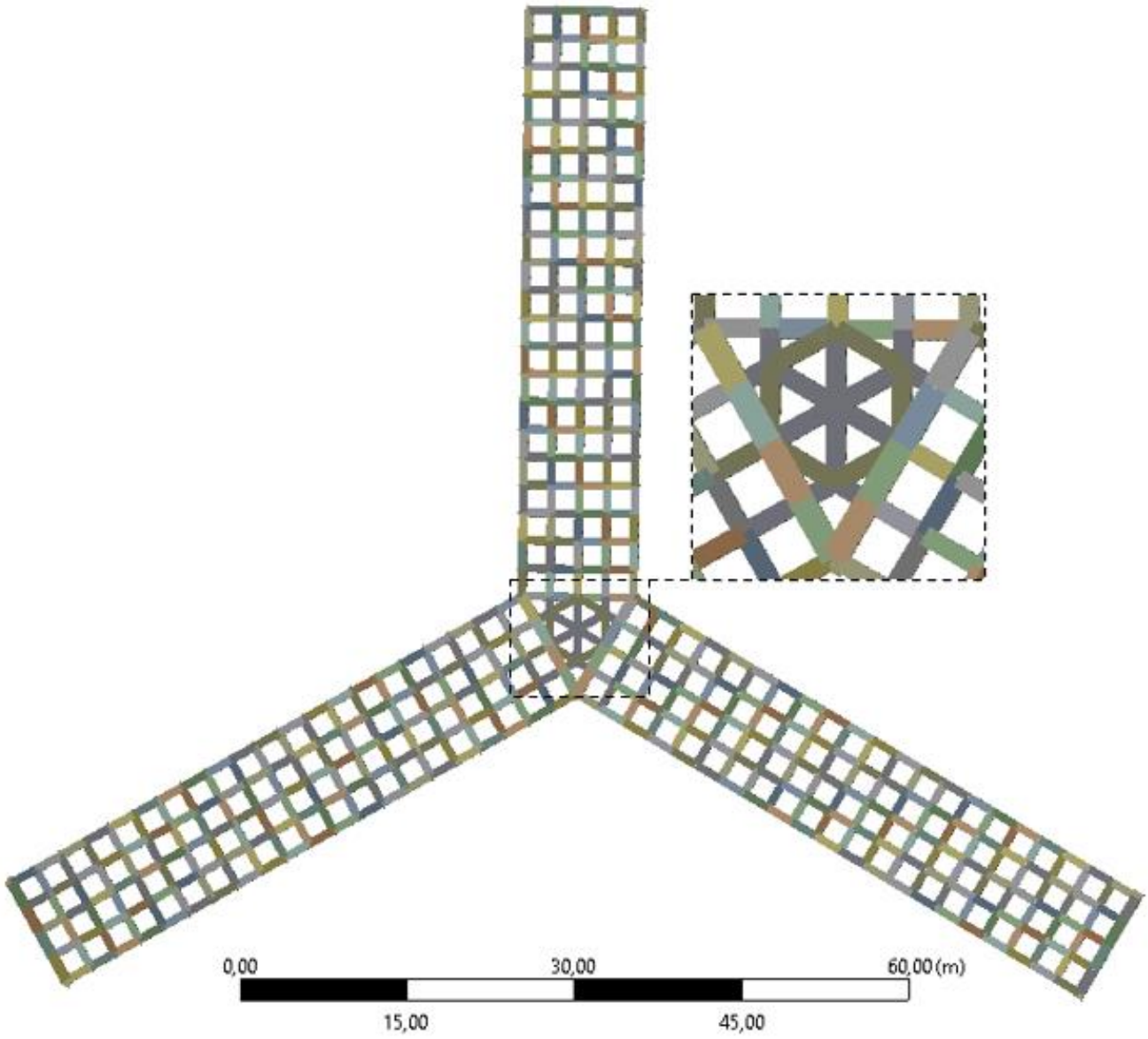

Figure 17: TLP top view

Chapter 5 Preliminary results

This chapter includes the results from the preliminary design. Shown in Table 12 below is the given added mass estimation and stiffness for the chosen concept design.

Table 12: Spreadsheet results.

	SURGE/ SWAY	**HEAVE**	**PITCH**	**SURGE-PITCH**	**YAW**
ADDED MASS	45032303,8	13992020,0	21316669869	335550332	$4{,}45E+09$
STIFFNESS	1147244,3	1986771096	$7{,}75608E+11$	38252567,99	$2{,}5E+09$

Table 13 provides the resulting values for the pretension calculation:

Table 13: Pretension.

$\boldsymbol{\nabla}\ [\boldsymbol{m^3}]$	$\boldsymbol{F_B}\ [\boldsymbol{N}]$	$\boldsymbol{F_t}[\boldsymbol{N}]$	$\boldsymbol{F_{pre}}[\boldsymbol{N}]$
$\mathbf{26908,49}$	270571576,9	41122709,1	102467343,4

The table above shows that the total pretension required for the TLP is 102,467MN.

The operating and towing conditions with respect to the two periods of interest: surge and heave, the calculated values are provided in Table 14.

Table 14: Natural period.

	OPERATING CONDITION	**TOWING CONDITION**
$\boldsymbol{T_{n1}[s]}$	111,014	108,426
$\boldsymbol{T_{n3}[s]}$	2,203	2,206

Given the criteria in Table 5, $T_{n1} > 100$s, and $T_{n3} < 5s$ in which satisfy the criteria.

Chapter 6 Global analysis

This chapter shows the results obtained from the global static analysis.

6.1. Beam stresses.

This chapter focuses on the global analysis of the structure, and here all the stresses are displayed. Firstly, displayed in Figure 18, the direct stress for the entire glulam system is shown. Here the max value reaches $38{,}46\ MPa$ and is located in the connected top beams of Pontoon 3 and the centre structure. The lowest value is negative $50{,}77\ MPa$, although this negative result is neglectable due to a fixed connection on pontoon 3. The average value for pontoons 1 and 2 is negative $11{,}11\ MPa$ as indicated by the colour bar.

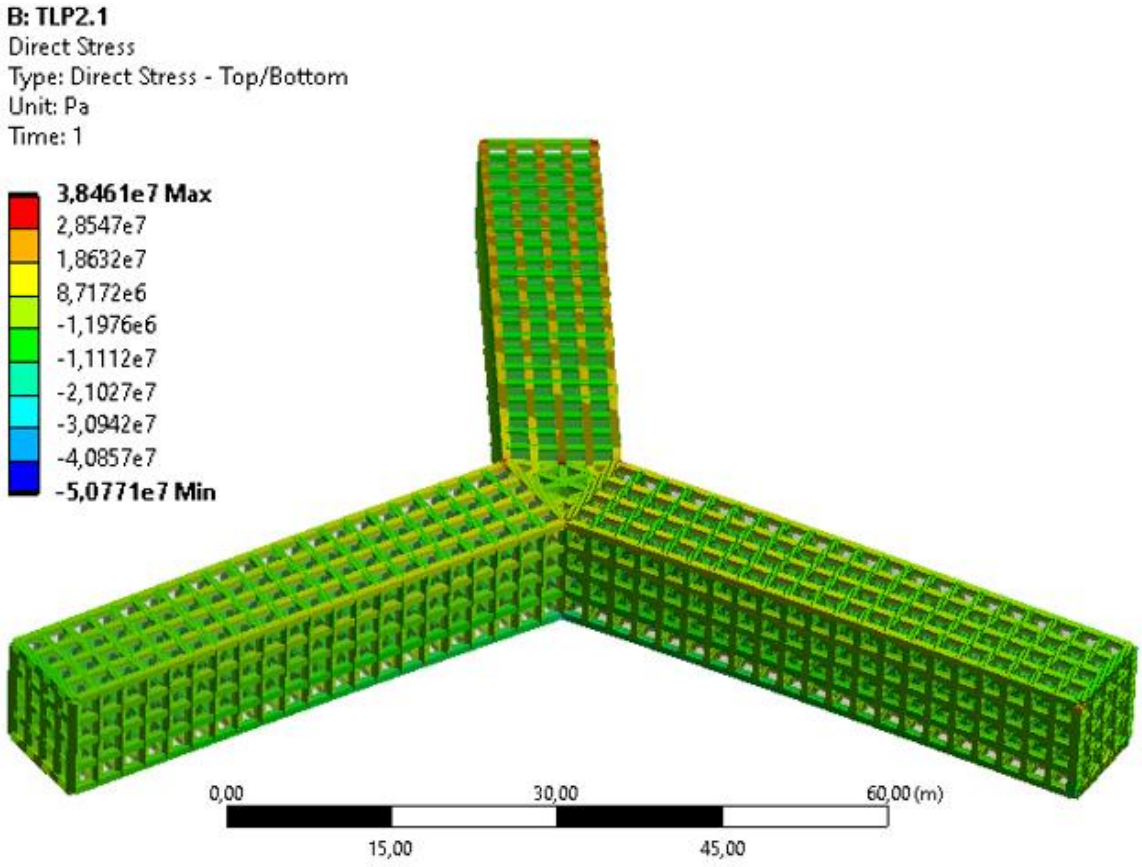

Figure 18: Direct stress.

The minimum combined stress is illustrated in Figure 19, with the maximum value on pontoon 3, and has a value of 34,82 MPa.

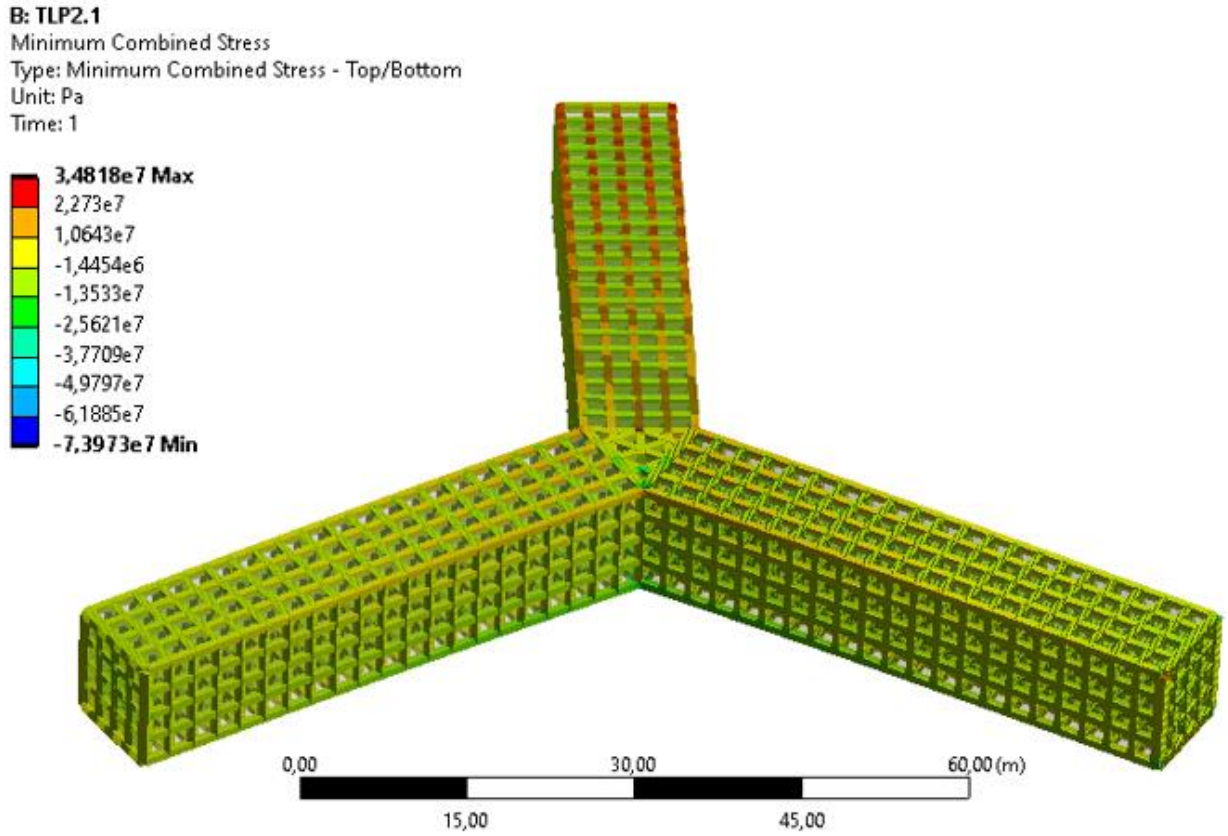

Figure 19: Minimum combined stress.

Maximum combined stresses are shown in Figure 20, and here both maximum and minimum values are neglected due to its location on pontoon 3 and centre structure, and the value of interest is 5,57 MPa.

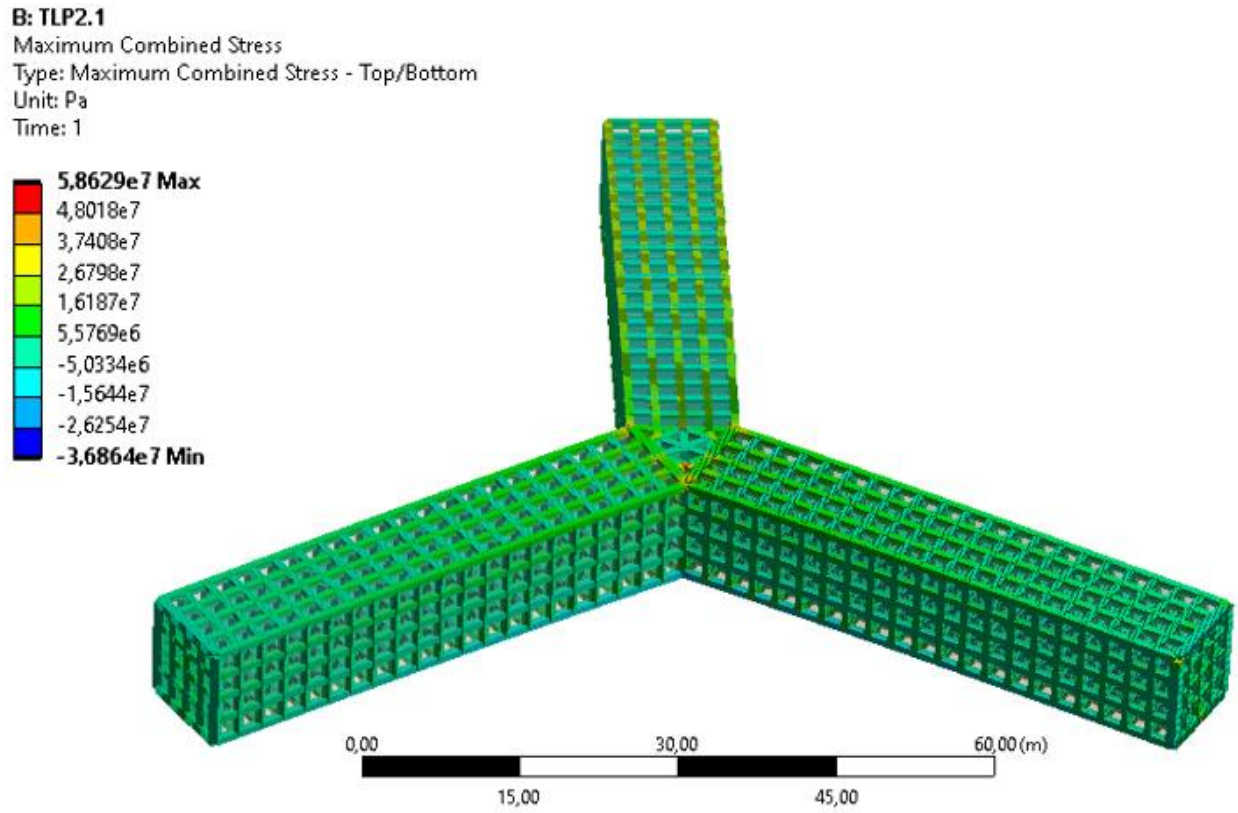

Figure 20: Maximum combined stress.

Equivalent stress is shown in Figure 21, and for the plate, the equivalent stress is $2{,}7\ x\ 10^{-2}\ MPa$.

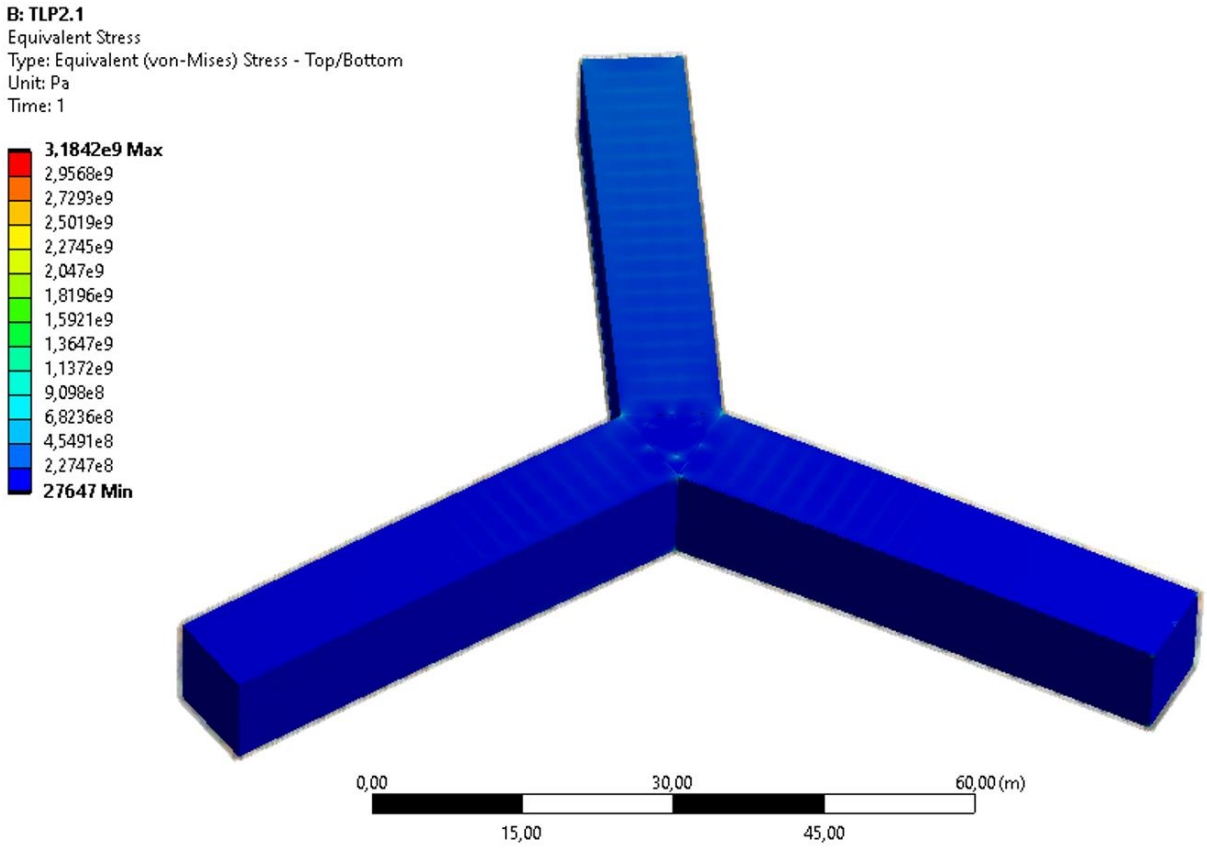

Figure 21: Eqvivaltent stress.

Deformation for the structure is hydrostatic pressure dominated, as shown in Figure 22. The pressure bends the plate inwards and drags the end of pontoons 1 and 2 downwards, resulting in a total deformation of $1{,}277m$. As the deformation should not exceed 5% of the total length, this is not an issue, as the total deformation is 1,2%.

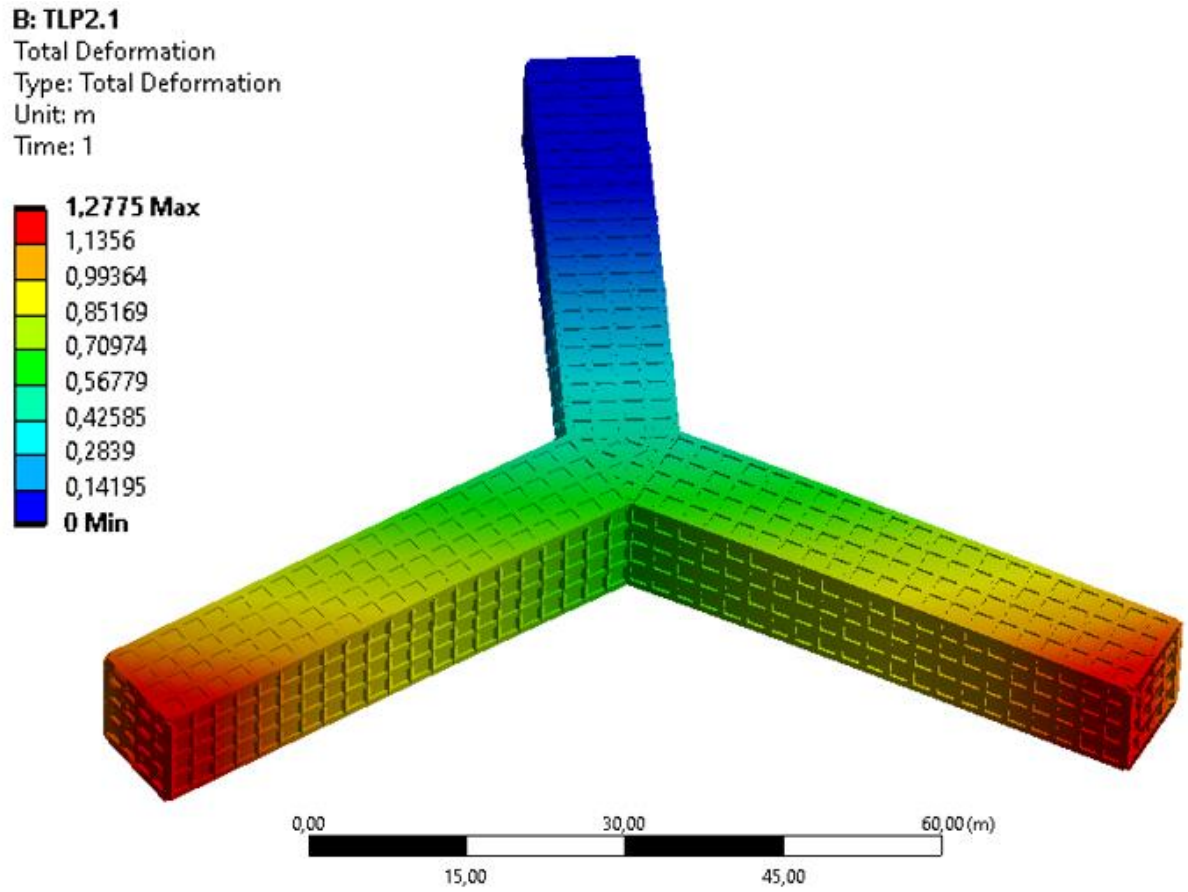

Figure 22: Total deformation.

Axial force on the global scale equals 1,73 MN, as shown in Figure 23, and has a maximum value of 39,4 MN located in the centre connection between Pontoon 1-3 and Pontoon 2-3.

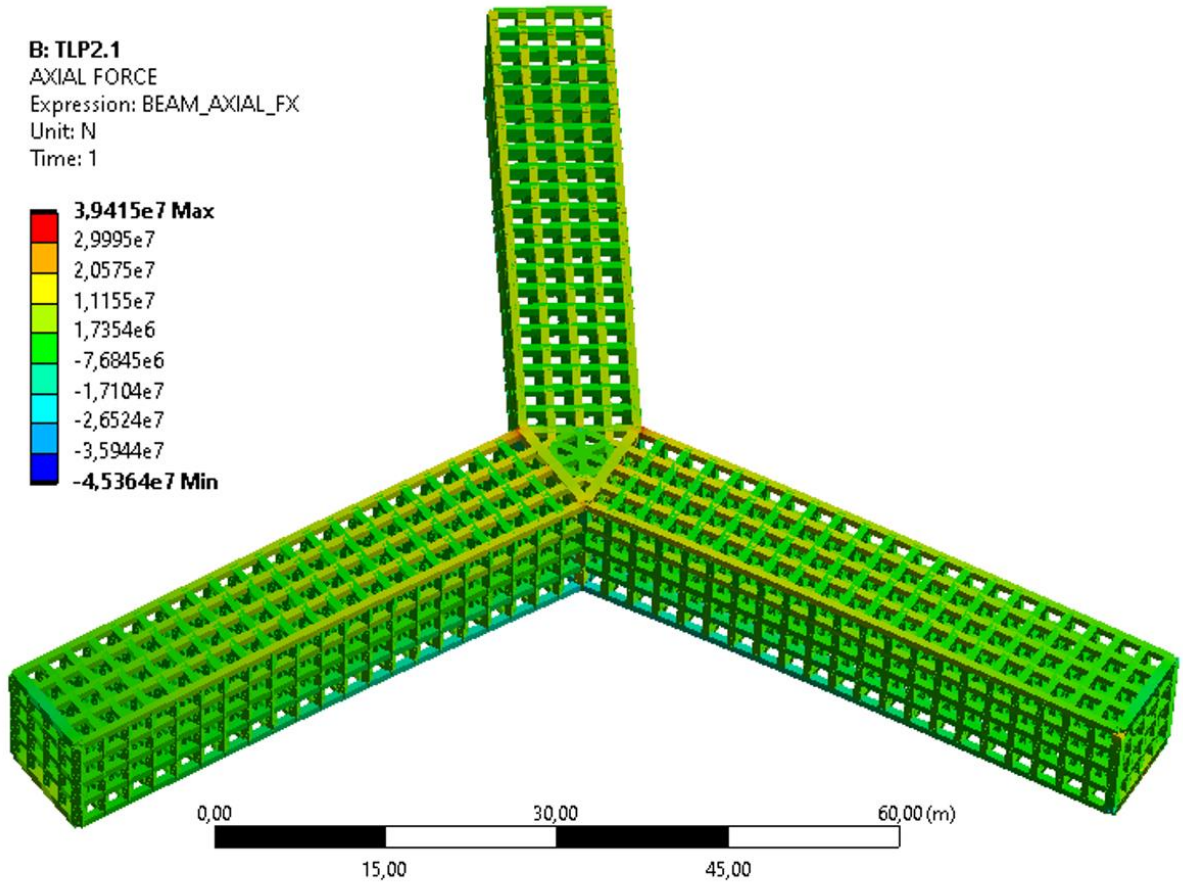

Figure 23: Axial force.

The bending moment around the y-axis is shown in Figure 24. The highest moment is due to the ridig body of the centre structure and equals $4{,}26\ MNm$, and through of the first and second pontoon, the moment equals $0{,}376\ MNm$.

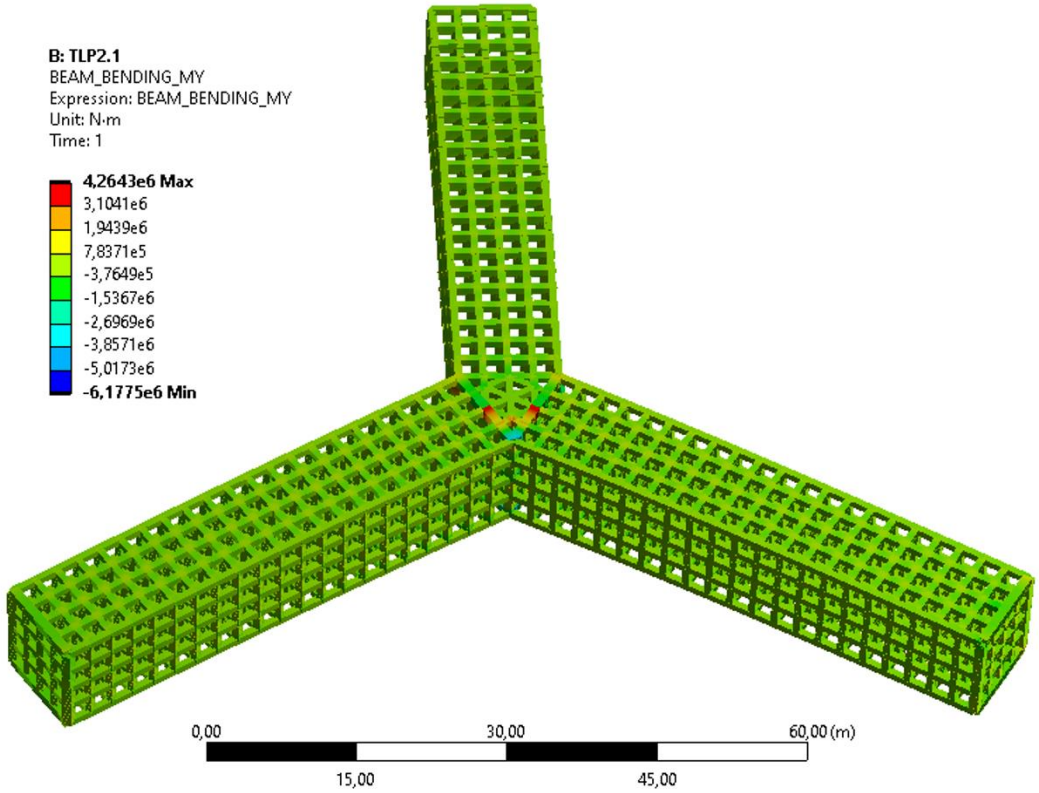

Figure 24: Bending moment M_y.

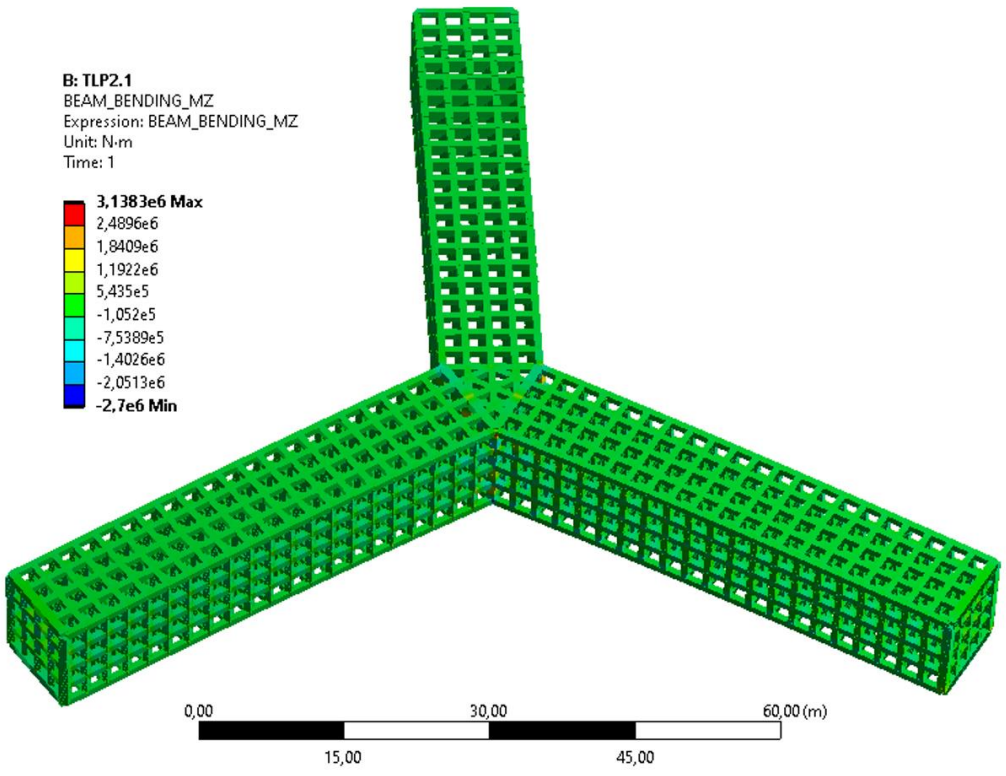

Figure 25: Bending moment M_z.

The offshore structure's stability is mainly preserved against torsional moment on the pontoons of the TLP. The pontoons on the TLP are engineered to lessen the effects of outside forces that try to twist the platform along its vertical axis. The configuration of the pontoons is designed to minimize the possibility of torsional forces by reducing drag and hydrodynamic effects. As a counterweight, the tendons holding the TLP to the seafloor provide stability by varying their tension in response to twisting forces, and the torsional moment on a global scale is illustrated in Figure 26.

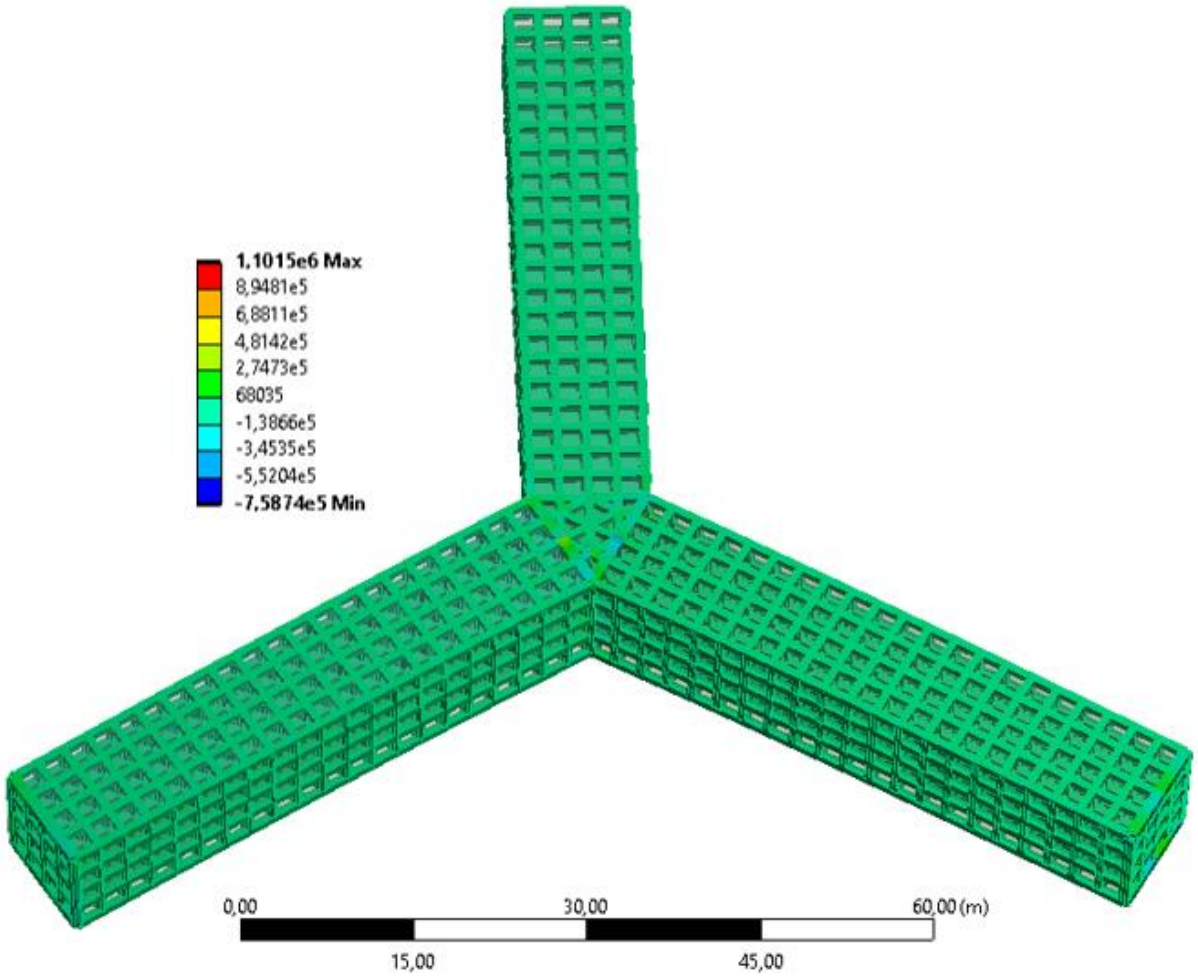

Figure 26: Torsional moment.

6.2. ULS timber results

This sub-chapter covers the ultimate limit state timber results on a global scale using the five criteria given in Chapter 3.3.1; the utilization factor is shown in Table 15. The utilization is highest when subjected to criteria 5, "stability". Calculated value for $\lambda_{m,rel}$ is 0,17, which gives $k_{crit} = 1$ and $k_{c,z} = 1{,}031$. Therefore, the utilization is taken as 85,6% which is considered acceptable. Complete illustrations from the analysis can be found in Appendix A.

Table 15: ULS Timber results.

	BENDING AND TENSION 1	**BENDING AND TENSION 2**	**BENDING AND COMPRESSION 1**	**BENDING AND COMPRESSION 2**	**STABILITY**
UTILIZATION [%]	53,47	75,36	64,8	66,75	52,22

6.3. ULS steel results.

The utilization for the steel plate is shown in Figure 27. The highest utilization for the steel plate 95,66%, shown by the colour bar and the colour indications of the model. As for the average, the value is 47,83% as indicated by the darker blue colour.

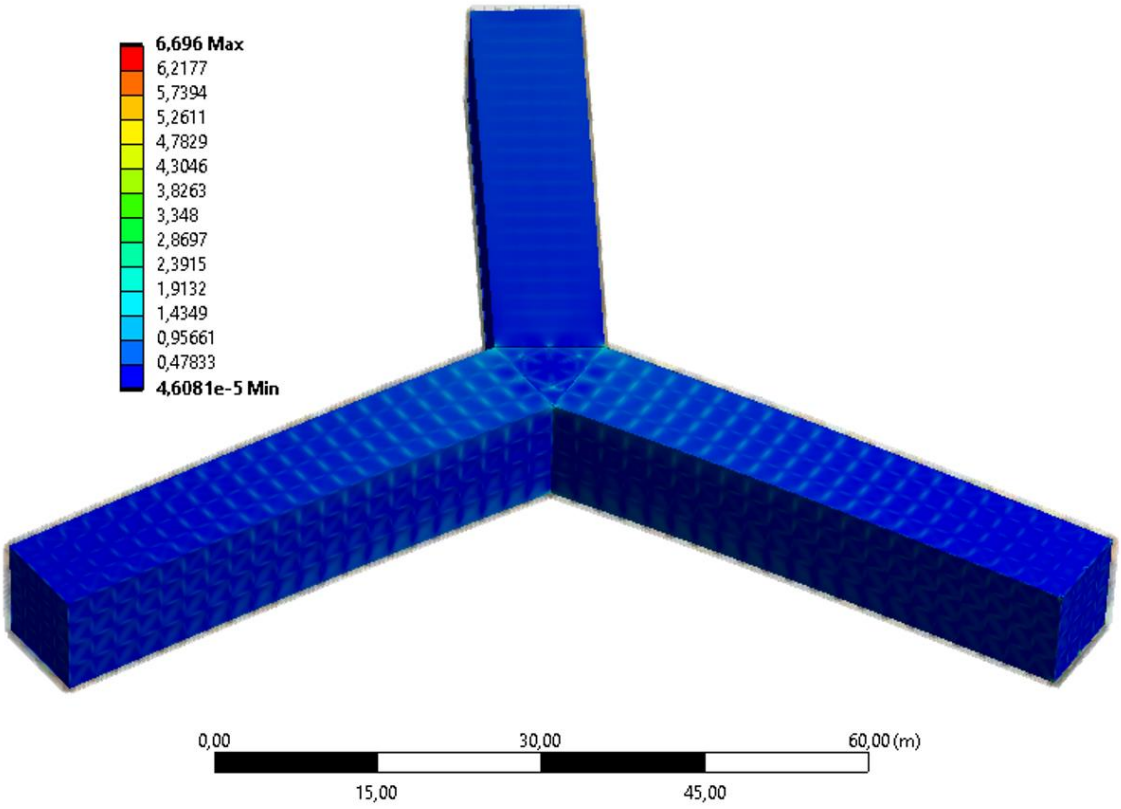

Figure 27: Steel plate utilization.

Chapter 7 Discussion

The following sub-chapters include the discussion on different aspects of this thesis, the discussion of the model, and the discussion of the main results obtained.

This thesis examined the concept design and global structural analysis for a TLP with three pontoons and a load-bearing structure made of glulam. The pontoons are covered with 50mm thick steel plating to ensure the structural frame is in a moisture-free environment. This thesis uses Excel for the initial spreadsheet calculations based on an existing design for a 5 MW TLPWT [3]. Examining the results from the spreadsheet calculations gave the foundation for upscaling the design and then finalizing the concept using ansys mechanical. This provided a concept design with acceptable static utilization because the base model had less than 5% variation in dynamic vs static loading; dynamic analysis was neglected here.

7.1. The model

This chapter focuses on the FEM model and its performance.

7.1.1. Assumptions

During this thesis, a concept design of TLP supporting a 15MW WT has been developed. Simplifications and assumptions were necessary during the development to obtain the static results.
One of these simplifications was adding a zero displacement on the end of the third pontoon, invalidating the third pontoon's result but making it possible to read the result for the remaining two pontoons. And by adding the thrust force in the worst possible direction (aligned with the third pontoon), the confidence for a statically stable structure was obtained. When adding the thrust force to the model, the connection to the centre structure had to be made rigid, introducing a rigid body motion to the system. This connection invalidated some results, explaining the high bending moment in the connective members, as shown in Figure 24.

Six design criteria provided in chapter 3.3 were added as functions to the model in Ansys to obtain the utilisation for both the timber structure and steel plating. Ansys does not separate tension from compression in other ways than positive and negative values. So when reading the results from criteria 3 and 4, when only subjected to compression, the results include some high values due to the tension force. By including the tension force in these criteria, a utilization is shown to be as high as 400% though this is neglected and has a few explanations. Firstly the results include both the rigid body of the centre structure; second, it contains the results from the third pontoon; and lastly, as mentioned earlier, the tension force. Starting with the spreadsheet design for the pontoon, an initial assumption was made for the density when using the volume of the base design. This value was calculated by taking the total weight of the timber in the initial pontoon design and dividing it by the total volume of the pontoon.

7.1.2. Decision variables and result

The main pontoon dimensions were identified as decision variables. Treating the TLP draft as input allows the engineer to try different concepts and configurations. And another approach would be to treat various drafts as variables. The pontoon's chosen variables (height, width and length) made it possible to make a configuration with natural period as an output. Then by looking at the output, the input could be chosen and further processed. As the main variables were the total height, width and length of the pontoon, the load-bearing system was not decided and needed a configuration. Initially chosen, it was a simple structure with a beam cross-section of 500 x 500 mm and cc 5000 mm. However, when adding the loads, the utilization was over 100%, resulting in a structural collapse. Then changing to cc 2500 mm, and it still got collapsed. So changing to a larger cross-section was done; now, mostly all the cross-sections were 750 x 750 mm and got a utilization of 53-62% for most of the members, but still over 100% on the end of the pontoons and closest to the centre construction. So the cross-section was made to be $1000x1000mm$ to ensure a safe and stable structure.

As the GL30h's compression strength, as shown in chapter 2.2.2, gives a high utilization factor in some areas, this can be seen as less attractive, but based on the fact that the strength can be higher than advertised shown by McConnel et al. [23] the utilization is acceptable.

The steel plate thickness was also a variable that needed a configuration and started with 40mm steel plating with a yield strength of 200MPa. The resulting utilization was way over an acceptable value, increasing the thickness. When a too-thick plate was realised, a change in the steel grade was the solution. The chosen steel grade was F690W, with a yield strength of 690 MPa, and ending up with a plate thickness of 50mm, giving utilization of 75%.

The natural periods for the concept design are taken as is; due to no dynamic analysis, this was not further investigated. The dynamic behaviour can be investigated when performing this analysis, and a more accurate behaviour can be obtained.

Chapter 8 Conclusion

The main objective of this thesis was to deliver a hybrid steel-glulam concept design for a tension-leg platform supporting a 15MW WT. Based on the discussion in the previous chapter, a concept design for a TLP was developed. This involved simplifying and making assumptions to obtain the hydro- and structural static results. These simplifications made results for the third pontoon invalid due to the zero displacement at the end. But due to symmetry, the concept design stands valid due to acceptable results for the first and second pontoons.

The main dimensions for the pontoon were identified as critical variables, allowing for the evaluation of different options. The output, which includes the natural period in both towing and operational conditions for the configuration, guides selection and further refines the input parameters.

When considering the load-bearing system, the initial configuration with a smaller cross-section and less considerable cc distance led to structural collapse due to excessive utilization. Adjustments were made by respectfully increasing the cross-section to 750 x 750mm and 1000 x 1000mm and decreasing the cc to 2500mm. This ensured a safe and statically stable structure.

The initial plate thickness of 40mm and steel grade with yield utilization of 200 MPa, when over the acceptable utilization and making the steel grade and thickness a crucial component of the TLP design. By changing to steel grade F690W, with a yield strength of 690 MPa, and increasing the thickness to 50mm, the plate problem was solved. The resulting and acceptable utilization was then 75%.

In conclusion, the concept design allowed for determining key parameters for the TLP design. The chosen pontoon dimensions, load-bearing system configuration and steel grade ensured a safe and statically stable structure.

Chapter 9 Further work

To enhance the understanding of the FOWT performance, a coupled and decoupled dynamic analysis is recommended. These analyses aim to investigate the dynamic interactions between the TLP and wind turbine and examine the behaviour of the TLP alone. By using this approach, valuable insight to guide design improvements is obtained.

It is crucial to use cutting-edge numerical modelling approaches for simulating the dynamic behaviour of the TLP and wind turbine for the coupled study. The intricate interplay between the two should be included in this study, as well as elements like wave-induced motions, wind loads, and the response of the TLP's mooring system. We can forecast the system's performance, including structural integrity and operational stability, by precisely capturing the link between the turbine's rotor dynamics and the TLP's structural reaction. We will be able to improve the design of the TLP and wind turbine using the results of this coupled study, aiming to maximize energy output while reducing structural stresses.

A decoupled analysis can be performed in addition to a coupled analysis to understand the separate parts better. This entails examining the TLP and wind turbine's activity independently. We may then carefully assess the unique properties and constraints of each component. For instance, we may analyse how the TLP reacts to environmental factors like waves and currents and the wind turbine's aerodynamic efficiency and load distribution. Using this decoupling analysis, we can determine which component designs need to be changed or enhanced to increase performance and reliability.
Additionally, it is critical to do a thorough tendon analysis to guarantee the reliability and effectiveness of the TLP's mooring mechanism. The tendons are essential for the platform's support, the transmission of loads from the wind turbine to the TLP's base, and maintaining its stability and position. A thorough investigation is required to improve the tendon system's design and performance.
This tendon study should include several variables, including the tendons' composition, configuration, and installation techniques. It should assess how the tendons behave mechanically under various loading scenarios, such as wave-induced movements, wind loads, and dynamic reactions. It is advised to use sophisticated numerical simulations like finite element analysis to predict the complicated behavior of the tendons correctly.

The tendon analysis should also consider elements like fatigue, corrosion, and wear that may impact the tendon's structural integrity and longevity. Environmental factors like seawater temperature and composition should be considered. We can identify possible failure modes and dangers by performing a thorough tendon analysis, and we can then put the right solutions in place to increase the mooring system's dependability and durability.

To summarise, coupled and decoupled studies for the TLP and wind turbine system and a thorough tendon analysis will yield useful information for enhancing the design, functionality, and dependability of TLPs in wind energy applications. The TLP-wind turbine system will become more efficient overall due to these assessments, which will also increase energy production and guarantee structural integrity.

References

1. Withee Jon E., Fully coupled dynamic analysis of a floating wind turbine system, (2004).
2. Equinor marks 5 years of operations at world's first floating wind farm, (2022).
3. E.E. Bachynski, Design and dynamic analysis of tension leg platform wind turbines, (2014).
4. D. Roddier, C. Cermelli, and A. Weinstein, WindFloat: A Floating Foundation for Offshore Wind Turbines—Part I: Design Basis and Qualification Process, *in American Society of Mechanical Engineers Digital Collection*, (2010): pp. 845–853.
5. C. Cermelli, D. Roddier, and A. Aubault, WindFloat: A Floating Foundation for Offshore Wind Turbines—Part II: Hydrodynamics Analysis, *in American Society of Mechanical Engineers Digital Collection*, (2010): pp. 135–143.
6. A. Aubault, C. Cermelli, and D. Roddier, WindFloat: A Floating Foundation for Offshore Wind Turbines—Part III: Structural Analysis, *in American Society of Mechanical Engineers Digital Collection*, (2010): pp. 213–220.
7. C. (Christopher H. Tracy, Parametric design of floating wind turbines, Thesis, Massachusetts Institute of Technology, 2007.
8. K.H. Lee, Responses of floating wind turbines to wind and wave excitation, Thesis, Massachusetts Institute of Technology, 2005.
9. E.N. Wayman et al., Coupled Dynamic Modeling of Floating Wind Turbine Systems, *in OnePetro*, (2006).
10. P. Dietsch and J. Köhler, *Assessment of Timber Structures*, (2010).
11. J.F. Wilson, *Dynamics of Offshore Structures*, *John Wiley & Sons*, (2003).
12. P. Manik et al., Technical and Economic Analysis of the Usages Glued Laminated of Apus and Petung Bamboo as an Alternative Material Component of Timber Shipbuilding, *Materials Today: Proceedings* 13 (2019) 115–120.
13. Y. Lu, P. Cui, and D. Li, Carbon emissions and policies in China's building and construction industry: Evidence from 1994 to 2012, *Building and Environment* 95 (2016) 94–103.
14. V.J.L. Gan et al., A comparative analysis of embodied carbon in high-rise buildings regarding different design parameters, *Journal of Cleaner Production* 161 (2017) 663–675.

15. B. Liu et al., A multi-regional input–output analysis of energy embodied in international trade of construction goods and services, *Journal of Cleaner Production* 201 (2018) 439–451.
16. L. Martin and F. Perry, Chapter 11 - Sustainable Construction Technology Adoption, *in* V.W.Y. Tam, K.N. Le (Eds.), Sustainable Construction Technologies, *Butterworth-Heinemann*, (2019): pp. 299–316.
17. S. Gold and F. Rubik, Consumer attitudes towards timber as a construction material and towards timber frame houses – selected findings of a representative survey among the German population, *Journal of Cleaner Production* 17 (2) (2009) 303–309.
18. J.P. Newell and R.O. Vos, Accounting for forest carbon pool dynamics in product carbon footprints: Challenges and opportunities, *Environmental Impact Assessment Review* 37 (2012) 23–36.
19. A.T. Balasbaneh and AK Bin Marsono, Strategies for reducing greenhouse gas emissions from residential sector by proposing new building structures in hot and humid climatic conditions, *Building and Environment* 124 (2017) 357–368.
20. A. Purkus et al., Towards a sustainable innovation system for the German wood-based bioeconomy: Implications for policy design, *Journal of Cleaner Production* 172 (2018) 3955–3968.
21. AK Bin Marsono and A.T. Balasbaneh, Combinations of building construction material for residential building for the global warming mitigation for Malaysia, *Construction and Building Materials* 85 (2015) 100–108.
22. T. Bowers et al., Cradle-to-Gate Life-Cycle Impact Analysis of Glued-Laminated (Glulam) Timber: Environmental Impacts from Glulam Produced in the US Pacific Northwest and Southeast*, *Forest Products Journal* 67 (5–6) (2017) 368–380.
23. Post-tensioning of glulam timber with steel tendons, *Construction and Building Materials* 73 (2014) 426–433.
24. A. Kutnar and C. Hill, Life Cycle Assessment – Opportunities for Forest Products Sector, *BioProducts Business* (2017) 52–64.
25. K. Pingoud and A. Lehtilä, Fossil carbon emissions associated with carbon flowsof wood products, *Mitigation and Adaptation Strategies for Global Change* 7 (1) (2002) 63–83.
26. T. Okada et al., Evaluating the durability of structural glulam bonded with aqueous polymer-isocyanate adhesive by two kinds of accelerated aging treatments, *Eur. J. Wood Prod.* 78 (1) (2020) 113–122.

27. R.V. Mendagaliyev et al., The influence of a protective environment during direct laser deposition on the formation of structure and properties of steel F690W (09CrNi2MoCu), *Materials Today: Proceedings* 30 (2020) 712–717.
28. A. Orlov et al., Mechanical properties prediction of the materials gained by combining additive technologies, *Materials Today: Proceedings* 30 (2020) 752–755.
29. DNV-RP-C205 Environmental conditions and environmental loads.pdf, (n.d.).
30. C.L. Kirk and E.U. Etok, Dynamic response of tethered production platform in a random sea state, *in* Proc. BOSS, (1979): pp. 1979–8.
31. Definition of the IEA 15-Megawatt Offshore Reference Wind Turbine.pdf, (n.d.).
32. G. Bywaters et al., Northern Power Systems WindPACT Drive Train Alternative Design Study Report: April 12, 2001 to January 31, 2005, (2004).
33. J. Jonkman et al., *Definition of a 5-MW Reference Wind Turbine for Offshore System Development*, (2009).
34. C. Bak, The DTU 10-MW Reference Wind Turbine, (2013).
35. Deliverable reports on INNWINDEU -, *Https://Www.Innwind.Eu* (n.d.).
36. C. Desmond et al., Description of an 8 MW reference wind turbine, *J. Phys.: Conf. Ser.* 753 (9) (2016) 092013.
37. D.T. Griffith and T.D. Ashwill, The Sandia 100-meter All-glass Baseline Wind Turbine Blade: SNL100-00, (n.d.).
38. P. Bortolotti et al., *IEA Wind TCP Task 37: Systems Engineering in Wind Energy - WP21 Reference Wind Turbines, National Renewable Energy Lab. (NREL), Golden, CO (United States)*, (2019).
39. Offshore wind in Europe Key Trends and Statistics, *WindEurope* (2019).
40. Y. Zhao, J. Yang, and Y. He, Preliminary Design of a Multi-Column TLP Foundation for a 5-MW Offshore Wind Turbine, *Energies* 5 (10) (2012) 3874–3891.
41. J. Großmann et al., The GICON®-TLP for wind turbines, (n.d.).
42. sw-design-of-timber-structures-vol3-2022.pdf, (n.d.).
43. sw-design-of-timber-structures-vol2-2022.pdf, (n.d.).
44. *Timber structures Glued laminated timber and glued solid timber Requirements:*, *BSI British Standards*, (n.d.).
45. SS-EN 1995-1-1 buckling factor 45.pdf, (n.d.).
46. H.J. Blaß and C. Sandhaas, Timber Engineering - Principles for design, (n.d.).
47. en1993152006.pdf, (n.d.).
48. NS-EN 1993-1-1.pdf, (n.d.).

49. NS-En-1993-1-5-Engelsk.pdf, (n.d.).
50. C. Moga et al., Aspects Regarding EC3-2 Procedure for Stability Verification of the Free-Standing Circular Arches, *Bulletin of the Polytechnic Institute of Iași. Construction. Architecture Section* 67 (3) (2022) 105–117.
51. J. Wu and M.-H. Kim, Generic Upscaling Methodology of a Floating Offshore Wind Turbine, *Energies* 14 (24) (2021) 8490.
52. A. Crozier, Design and Dynamic Modeling of the Support Structure for a 10 MW Offshore Wind Turbine, Master thesis, Institutt for energi- og prosessteknikk, 2011.

Appendix A

Figure 28 to Figure 33 shows the resulting utilization for the specific design criteria.

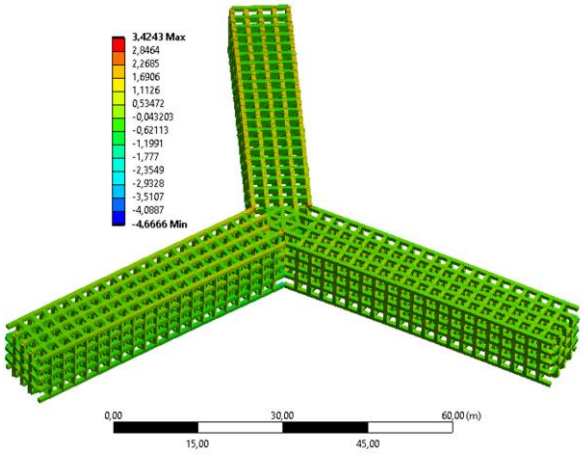

Figure 28: Criteria 1.

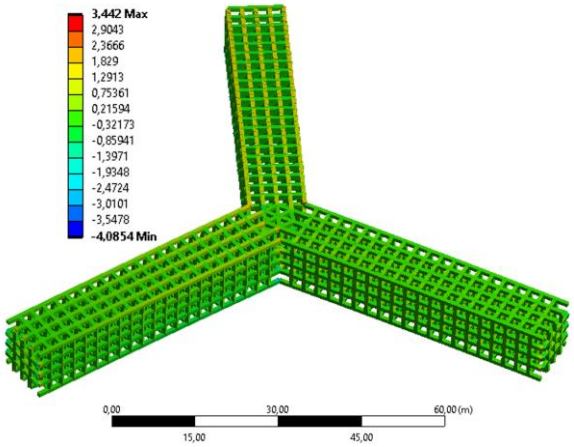

Figure 29: Criteria 2.

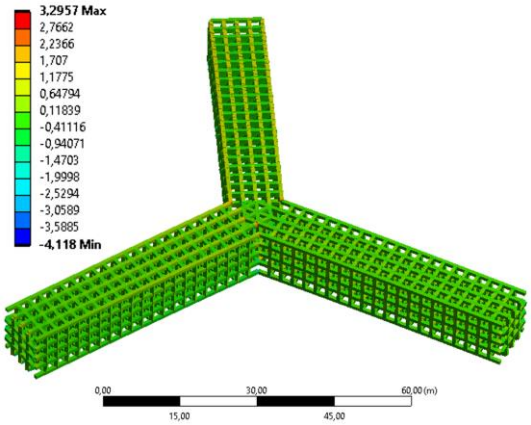

Figure 30: Criteria 3.

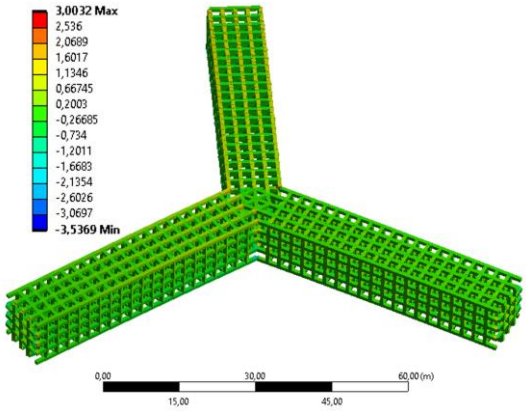

Figure 31: Criteria 4.

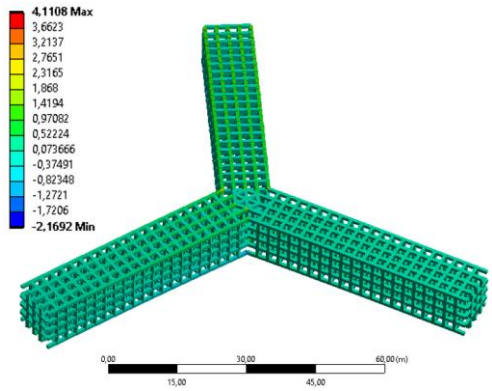

Figure 32: Criteria 5.

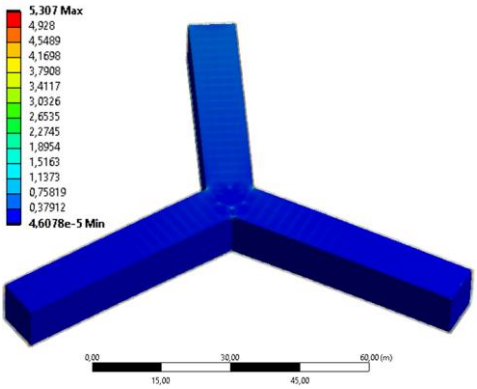

Figure 33: Criteria 6.

Results from spreadsheet calculations are shown in the tables below.

	ρ_W	T	r_p	w_p	h_p	b_t	D_1	D_2	l_p
TLP 2	1025,00	35	32	5	5	10	14	14	25
TLP 3	1025,00	22	28	6	6	10	14	14	21
TLP 4	1025,00	29	25	6	6	10	7	10	20
TLP 2 WOOD	1025,00	35	32	5	5	10	14	14	25
CONCEPT TLP	**1025,00**	**60**	**52**	**10**	**10**	**15**	**23**	**23**	**42**
TLP 3, UPSCALED	1025,00	38	47	10	10	15	23	23	35
TLP 4, UPSCALED	1025,00	50	42	10	10	15	11	17	33

	$h1$	$h2$	A_w	n_p	z_s	$d_t\ [m]$	$t_t\ (mm)$	A_t	V_{C1}
TLP 2	40	5	154	3	-33	1,1	36,30	0,95	154
TLP 3	26	6	154	3	-19	1,3	42,90	1,33	154
TLP 4	33	6	33	4	-26	1,2	39,60	1,13	33
TLP 2 WOOD	40	5	154	3	-33	1,1	36,30	0,95	154
CONCEPT TLP	**67**	**8**	**428**	**3**	**-56**	**1,8**	**0,06**	**0,34**	**428**
TLP 3, UPSCALED	43	10	428	3	-33	2,2	0,07	0,47	428
TLP 4, UPSCALED	55	10	92	4	-45	2,0	0,07	0,40	92

	V_{C2}	V_P	m_{C1}	m_{C2}	m_P	$Weight\ TLP\ [kg]$	$Total\ weight[kg]$
TLP 2	154	1875	26255	26255	319807	372318	2626318
TLP 3	154	2268	26255	26255	386839	439350	2693350
TLP 4	79	2880	5660	13396	491224	510279	2764279
TLP 2 WOOD	154	1875	26255	26255	319807	372318	2626318
CONCEPT TLP	**428**	**8686**	**72961**	**72961**	**1481477**	**1627400**	**3881400**
TLP 3, UPSCALED	428	10506	72961	72961	1791995	1937917	4191917
TLP 4, UPSCALED	218	13341	15728	37225	2275549	2328502	4582502

ADDED MASS INITIAL PROPERTIES	PONTOON	UPPER COLUMN	NODAL COLUMN
	$a_t(h)$	$a_t(D1)$	$a_t(D2)$
TLP2	30455,31	157781,8375	157781,8375
TLP3	43855,65	157781,8375	157781,8375
TLP4	43855,65	34011,64609	80500,9375
CONCEPT TLP	**84631,93**	**438458,2126**	**438458,2126**
TLP 3, UPSCALED	121870	438458,2126	438458,2126
TLP 4, UPSCALED	121870	94514,5892	223703,1697

	SURGE	HEAVE	PITCH	SURGE-PITCH	YAW	HEAVE-DAMPING
	A11 [kg]	A33 [kg]	A55 [kg]	A51 [kg]	A66 [kg]	C33
TLP2	9563078	3020463,679	3803184952	188022654	434079569	1547839,826
TLP3	7692734	3499221,192	2124778312	115459715	345977223	1547839,826
TLP4	7471810	3776788,458	1467901012	133843542	438556500	333654,2482
CONCEPT TLP	**45032304**	**13992020**	**2,07155E+14**	**2,1999E+13**	**5587883517**	**4301275,066**
TLP 3, UPSCALED	39453818	16209820,11	21316669869	335550332	4453746637	4301275,066
TLP 4, UPSCALED	47104526	17495624,93	2,00383E+14	2,7233E+13	5645514814	927188,1201

STIFFNESS

	k_{11} $[N/m]$	k_{33} $[N/m]$
TLP2	99277,2	1336760608
TLP3	84562,2	1867045808
TLP4	56178,6	1590855600
CONCEPT TLP	**512336,7**	**474160360,3**
TLP 3, UPSCALED	382414,8	662257032,1
TLP 4, UPSCALED	185304,4	564290015,5

SURGE	**HEAVE**	**PITCH-SURGE**	**SURGE-PITCH**	**ROLL**	**PITCH**	**YAW**
$K11$ $[N/m]$	$K33$ $[N/m]$	$K51$ $[N]$	$K15$ $[N]$	$K44$ $\left[\frac{Nm}{rad}\right]$	$K55$ $\left[\frac{Nm}{rad}\right]$	$K66$ $[Nm]$
297831	4010281825	9679527	9679527	3,35671E+12	3,35671E+12	304979558
253686	5601137425	4820045,4	4820045,4	3,58928E+12	3,58928E+12	198890294
224714	6363422400	5842574,4	5842574,4	3,25082E+12	3,25082E+12	140446500
1537010	**1422481081**	**85838174,41**	**85838174,41**	**7,25957E+11**	**7,25957E+11**	**4373688936**
1147244	1986771096	38252567,99	38252567,99	7,75608E+11	7,75608E+11	2499442704
741217	2257160062	33363683,68	33363683,68	7,02521E+11	7,02521E+11	1287350784

TENSION

	∇ $[m^3]$	F_B $[N]$	F_t $[N]$	F_{pre} $[N]$
TLP 3, UPSCALED	26908,49	270571577	41122709,13	76482955,91
CONCEPT TLP	**34358,03**	**345478561**	**38076530,69**	**102467343,4**
TLP 4, UPSCALED	19213,63	193197852	44954344,98	37060876,75

	OPERATING CONDITION				**TOWING**			
	T_{n1} $[s]$	T_{n3} $[s]$	ω_1 $[Hz]$	ω_3 $[Hz]$	T_{n1} $[s]$	T_{n3} $[s]$	ω_1 $[Hz]$	ω_3 $[Hz]$
TLP 3, UPSCALED	121,3793	1,9920	0,0518	3,1541	118,2035	1,9942	0,0532	3,1507
CONSEPT TLP	**111,0142**	**2,2026**	**0,0566**	**2,8526**	**108,4262**	**2,2059**	**0,0579**	**2,8483**
TLP 4, UPSCALED	164,3310	1,9459	0,0382	3,2289	160,7079	1,9463	0,0391	3,2282